Geosynchronous Satellite Maneuver Classification and Orbital Pattern Anomaly Detection via Supervised Machine Learning

by

Thomas González Roberts

A.B., Astrophysical Sciences, Princeton University (2016)

Submitted to the Department of Aeronautics and Astronautics and
the Institute for Data, Systems, and Society

in partial fulfillment of the requirements for the degrees of

Master of Science in Aeronautics and Astronautics
and
Master of Science in Technology and Policy

at the
MASSACHUSETTS INSTITUTE OF TECHNOLOGY

June 2021

Author .....
Department of Aeronautics and Astronautics and
the Institute for Data, Systems, and Society
May 18, 2021

Certified by .....
Richard Linares
Charles Stark Draper Assistant Professor, Aeronautics and Astronautics
Thesis Supervisor

Accepted by .....
Zoltan Spakovszky
Professor, Aeronautics and Astronautics
Chair, Graduate Program Committee

Accepted by .....
Noelle Eckley Selin
Associate Professor, Institute for Data, Systems, and Society and
Department of Earth, Atmospheric and Planetary Sciences
Director, Technology and Policy Program

Geosynchronous Satellite Maneuver Classification and Orbital Pattern Anomaly Detection via Supervised Machine Learning

by

Thomas González Roberts

Submitted to the Department of Aeronautics and Astronautics and
the Institute for Data, Systems, and Society
on May 18, 2021, in partial fulfillment of the
requirements for the degrees of
Master of Science in Aeronautics and Astronautics
and
Master of Science in Technology and Policy

Abstract

Due to the nature of the geosynchronous (GEO) orbital regime, where space objects orbit the Earth once per sidereal day, GEO satellites can appear fixed to a position in the sky when observed from the Earth's surface. This unique orbital characteristic makes GEO satellites ideal for telecommunications missions that require Earth-fixed antennas to send and receive signals, such as television broadcasts or military communications. To maintain their position relative to the Earth's surface, GEO satellites must station-keep, or regularly expend onboard propellant to counteract the natural forces in the near-Earth space environment that perturb their orbital trajectories. Less frequently, GEO satellites perform maneuvers to alter their orbital characteristics more drastically. One such maneuver is a longitudinal shift: changing a GEO satellite's sub-satellite point from one position on the Earth's equator to another. Such a maneuver often requires both a series of impulsive thrusts and a period of natural drift.

This work describes an approach for detecting the components of longitudinal shift maneuvers—including the patterns associated with initiating and ending eastward and westward drifts—using convolutional neural networks trained on publicly available two-line element (TLE) data from the U.S. Space Command's (SPACECOM) space object catalog. A method for converting TLE data to geographic position histories—longitude, latitude, and altitude positions over time in the Earth-centered, Earth-fixed geographic reference frame—and labeling longitudinal shift maneuvers by inspection is described. A preliminary maneuver detection algorithm is designed, trained, and tested on all GEO satellites in orbit from January 1 to December 31, 2020. Performance metrics are presented for algorithms trained on two different training data sets corresponding to five and ten years' worth of geographic position time-histories labeled with longitudinal shift maneuvers.

When detected, longitudinal shift maneuvers can be used to identify anomalous behavior in GEO. In this work, a satellite's behavior is considered nominal if it adheres to the

satellite's pattern of life (PoL)—its previous on-orbit behavior made up of sequences of both natural and non-natural behavioral modes, including routine station-keeping, other on-orbit maneuvers, and uncontrolled motion—and anomalous if it deviates from the satellite's PoL. Identifying anomalous satellite behavior is of critical interest to space situational awareness (SSA) system operators, who may choose to task their sensors to obtain more observations of anomalous behavior, and satellite operators themselves, who may wish to diagnose its root cause. Applications of this work for international space policymaking, including the development of on-orbit norms of behavior and the distribution of spectral and physical space in GEO, is also discussed.

Thesis Supervisor: Richard Linares
Title: Charles Stark Draper Assistant Professor, Aeronautics and Astronautics

Acknowledgments

This work was made possible by the support I have received from colleagues, friends, and family.

To my advisor, Professor Richard Linares, thank you for welcoming me into your group and giving me the freedom to develop my research interests, while honing the skills I need to explore them. To my colleagues at the Astrodynamics, Space Robotics, and Controls Laboratory, thank you for the guidance and mentorship you have given me during my first two years at MIT; I have learned as much from you as I have from any textbook. To the faculty and staff at the Department of Aeronautics and Astronautics and Technology and Policy Program, thank you for offering me the flexibility and guidance I needed to develop a degree program on my terms that would prepare me for success in my doctoral work. To my colleagues and friends at the Center for Strategic and International Studies, thank you for forever giving me a new context to understand some of the biggest problems facing the international space community and the drive to solve them.

This work was proposed, developed, and written in its entirety during the COVID-19 global pandemic. During this time, I have come to appreciate my friends and family more than ever before. To my friends—new and old, near and far—thank you for the joy and confidence you give me; I do not always realize how much I need it. To my parents, thank you for instilling in me a love of teaching and learning. To my sisters, thank you for being life-long role models, no matter if you are across the country or down the street. To my aunt, uncle, and grandparents, thank you for the love, advice, and endless support you have given me over these past two years in Cambridge; I treasure the time we have spent together. I can not imagine what it would have been like to endure this historic era without the support I find in my friends and family.

And lastly, to Grace, my partner and best friend, thank you for the unconditional love you have given me all these years. Your strength, selflessness, and passion for doing what is right has taught me more than any degree program ever could.

Contents

List of Figures

List of Tables

THIS PAGE INTENTIONALLY LEFT BLANK

Chapter 1

Introduction

The geostationary belt—an invisible ring that surrounds the Earth 35,786 kilometers above its equator—is one of the most prized orbital regimes in the near-Earth space environment. Space objects placed precisely in the geostationary belt orbit the Earth once every 23 hours, 56 minutes, and 3.93 seconds, the same period over which the Earth rotates about its rotational access, known as one *sidereal day* [36]. This particular orbital period allows geostationary satellites to appear fixed to a position in the sky to observers on the ground: directly overhead for those on the Earth's equator and in the southern or northern sky for those observing from the northern or southern hemispheres, respectively. This unique orbital characteristic makes the geostationary belt ideal for telecommunications satellites that require Earth-fixed antennas to send and receive signals, such as television and radio broadcasting or military communications satellites.[1]

Not all objects that orbit the Earth with a period of one sidereal day are geostationary. Objects that have an orbital period of one sidereal day, but follow orbital trajectories with some eccentricity or inclination are known as *geosynchronous* satellites. Geosynchronous satellites do not appear perfectly fixed to observers on the ground, but instead can be observed tracing periodic patterns in the sky over the course of one day, as shown in Figure 1-1. When observed from the ground, satellites in geosynchronous orbit pass through the same positions in the sky at approximately the same time each day.

To maintain their position relative to the Earth's surface, satellites in the geosynchronous region (GEO) must expend onboard propellant—using a process known as *station-keeping*—to counteract the natural forces in the near-Earth space environment, known as

[1]Next time you take a walk in your neighborhood, take note of the dish-shaped antennas fixed to buildings. They always point the same direction in the sky to receive a satellite TV signal over the course of a day, despite the fact that the Earth is turning and only a fraction of the sky is visible at different times.

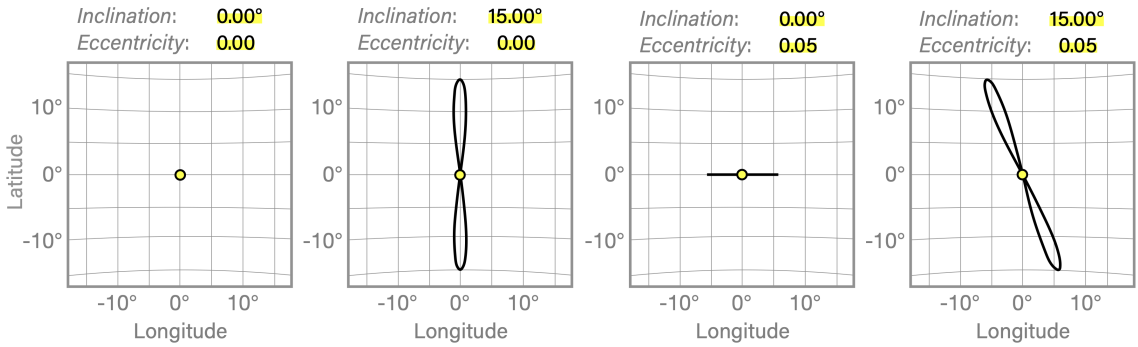

Figure 1-1: Geostationary and geosynchronous space object orbital patterns in Earth-centered, Earth-fixed geographic coordinates. This figure shows the simulated orbital trajectories of four geosynchronous space objects as observed in an Earth-centered, Earth-fixed geographic reference frame from a position on the Earth's equator over the course of one sidereal day. In this coordinate system, the origin (0°, 0°) corresponds to the observer's *zenith*, the position in the sky directly overhead. The vertical and horizontal axes are measured in degrees latitude and longitude from the zenith direction, respectively. Objects in geostationary orbit, like the one shown in the first subplot, appear fixed to a position in the sky. Objects in geosynchronous orbit, like those shown in the second, third, and fourth subplots, do not appear stationary in the sky, but rather trace out distinct patterns centered at the celestial equator. The movement between latitude and longitude extrema in the second, third, and fourth subplots is known as *libration* [24].

perturbation forces or simply *perturbations* [56]. Unlike satellites at lower orbital altitudes, GEO satellites are not primarily perturbed by atmospheric drag, but rather forces associated with the non-uniformity of Earth's gravitational field, the Sun and Moon's gravity, and solar radiation [49, 68]. Due to the magnitude of these perturbations, GEO satellites must perform station-keeping maneuvers frequently—on the order of once per week to several times per year for high-thrust chemical propulsion systems—in order to stay within a few fractions of a degree (in both the longitude and latitude directions) from their operator's desired position [9].

Less frequently, GEO satellites perform maneuvers to alter their orbital characteristics more drastically. One such maneuver—known as a *longitudinal shift*—is associated with changing a GEO satellite's sub-satellite point from one position on the Earth's equator to another. Such a maneuver often requires a series of impulsive thrusts to first remove the satellite from its initial position within the geostationary belt, allow it to naturally drift either eastward or westward around the belt, and finally reposition itself at a new longitudinal position.

An operator may choose to perform a longitudinal shift maneuver for a variety of reasons. A military operator may choose to shift a GEO satellite's sub-satellite point to alter

its observable region in response to a changing threat environment on the ground. A commercial communications operator may wish to better accommodate an unexpected change in customers' regional demands. If a GEO satellite is part of a *constellation*—a network of two or more satellites that work cooperatively to meet a set of mission requirements—its operator may choose to reposition it in conjunction with other aspects of the constellation's operational evolution, such as the retirement or addition of another satellite in the network. Lastly, an operator may choose to initiate an eastward or westward drift—the first component of a traditional longitudinal shift maneuver—as a means of retiring a satellite from service, since initiating an eastward or westward drift corresponds to lowering or raising the satellite's orbital altitude, respectively, a concept that will be discussed in Subsection 1.1.1.

1.1 Longitudinal Shifts

Unlike satellite maneuvers in other orbital regimes, which are often identified through discontinuities observed over time in one or more of the classical orbital elements—eccentricity, semi-major axis, inclination, right ascension of the ascending node, or argument of periapsis—longitudinal shifts in GEO can be detected by human inspection of time-series geographic position data. The following subsection demonstrates the discernible nature of longitudinal shift maneuvers in such datasets with an example.

1.1.1 Identifying Maneuvers in Time-Series Geographic Position Data

Figure 1-2 describes the geographic position of *Nimiq 2* (Satellite ID: 27632)—a GEO satellite operated by Telesat, a Canadian telecommunications company—from January 1 to December 31, 2015.[2] The first subplot, which depicts the satellite's longitudinal position over time, clearly shows that it began the year performing station-keeping maneuvers to maintain a sub-satellite longitude of approximately 109.1°W, an ideal position for offering coverage of the continental United States and Canada. Then, in mid-February, it initiated a longitudinal shift maneuver, which resulted in an eastward drift period that lasted until early May, highlighted in yellow in the figure.

During this drift period, the satellite orbited the Earth at a significantly lower orbital altitude than during the prior station-keeping period, as shown in the third subplot of Figure 1-2. Recall the equation of a satellite's velocity in a circular Earth orbit, v, as a

[2]The name, SPACECOM catalog ID number, launch date, and operator for each GEO satellite referenced in this work can be found in Appendix B.

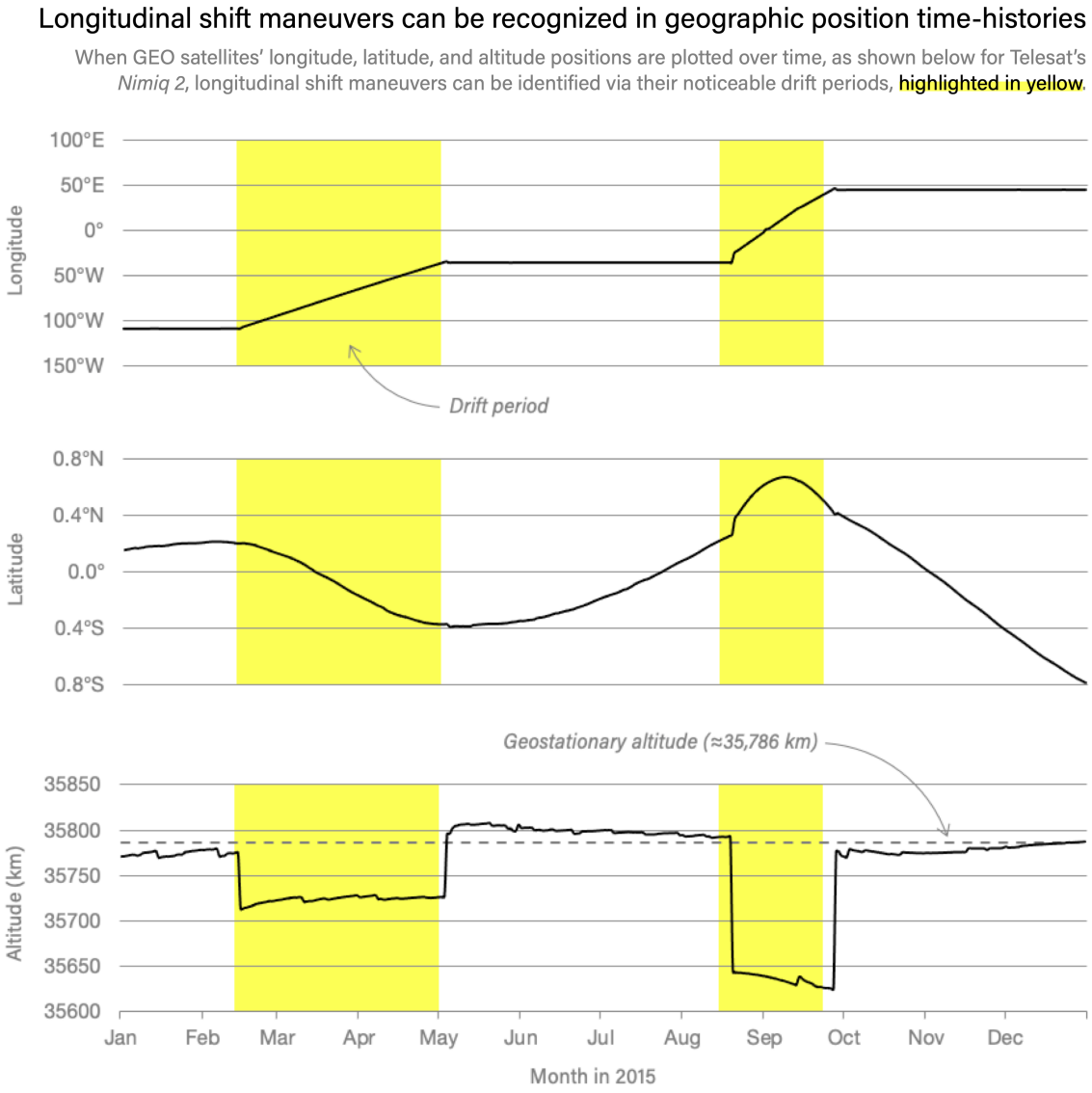

Figure 1-2: Geographic position time-history for Telesat's *Nimiq 2*. This figure shows daily positions in geographic coordinates—longitude, latitude, and altitude—for Telesat's *Nimiq 2* (Satellite ID: 27632) from January 1 to December 31, 2015. During this time, the satellite performed two eastward longitudinal shift maneuvers. These shift maneuvers produced two corresponding drift periods, highlighted in yellow. In each case, the satellite lowered its orbital altitude below geostationary altitude (≈35,786 km, shown with a dotted line in the third subplot), which resulted in a faster orbital velocity than other satellites in the geostationary belt and an eastward drift in longitude space, as shown in the first subplot.

function of its altitude, z [8]:

$$v = \sqrt{\frac{\mu_\oplus}{R_\oplus + z}} \tag{1.1}$$

where $\mu_\oplus$ is the Earth's gravitational parameter ($\approx$398,600 km^3/s^2) and $R_\oplus$ is the Earth's radius ($\approx$6,378 km). When z decreases, v increases: the satellite's orbital velocity was faster during the drift period than it was when it was station-keeping at one particular longitudinal position.[3] Since satellites in GEO traditionally orbit the Earth in an eastward direction—known as *prograde* motion—an increase in orbital velocity results in an eastward drift in geographic longitude, or a positive slope in the first subplot of Figure 1-2.

At the end of the first drift period, the satellite performed a second maneuver to end the eastward drift, and resumed station-keeping at a longitudinal position of approximately 36.0°W, with a sub-satellite point near the eastern coast of Brazil. The satellite maintained this position via station-keeping until mid-August, when it performed another longitudinal shift maneuver and initiated a second eastward drift.

In the third subplot of Figure 1-2, it is clear that this second eastward drift period was associated with an even lower orbital altitude than the first. Equation 1.1 tells us that a lower orbital altitude corresponds to faster prograde motion. This faster prograde motion led *Nimiq 2* to drift eastward faster than before as shown in the steeper, more positive slope in the satellite's longitudinal position over time in the first subplot of Figure 1-2. The second drift period ended when the satellite again performed a maneuver to end the eastward drift in late September, at which point it resumed station-keeping at a longitudinal position of 44.5°E over east Africa and the Arabian peninsula.

Although the satellite's altitude history offers an explanation for the changes observed in its longitude over time, its longitudinal position history alone is sufficient to identify the beginning and end of each longitudinal shift maneuver. Similarly, the latitudinal position history can be used to confirm longitudinal shift maneuvers, but is not critical—and often not sufficient—to discern such maneuvers when longitudinal position histories are also available.

1.1.2 Components of a Longitudinal Shift Maneuver

Both of the longitudinal shift maneuvers shown in Figure 1-2 are made up of two components associated with initiating and ending an eastward drift, which will henceforth be abbreviated

[3] Although Equation 1.1 describes the orbital velocity, v, of a space object in a *perfectly circular* orbit, it can be used as an approximation for objects in *nearly circular orbits*, which is the case for most GEO satellites before, during, and after a longitudinal shift maneuver.

Maneuver Type	Abbreviation	Description
Initiate Eastward Drift	**IE**	The maneuver associated with beginning a longitudinal drift with a positive slope that exceeds a specified duration threshold
End Eastward Drift	**EE**	The maneuver associated with ending a longitudinal drift with a positive slope that exceeded a specified duration threshold
Jump Eastward	**JE**	The maneuver associated with beginning and ending a longitudinal drift with a positive slope within a specified duration threshold
Initiate Westward Drift	**IW**	The maneuver associated with beginning a longitudinal drift with a negative slope that exceeds a specified duration threshold
End Westward Drift	**EW**	The maneuver associated with ending a longitudinal drift with a negative slope that exceeded a specified duration threshold
Jump Westward	**JW**	The maneuver associated with beginning and ending a longitudinal drift with a negative slope within a specified duration threshold

Table 1.1: The six components of longitudinal shift maneuvers. While some longitudinal shift maneuvers are made up of just one of the components listed above (JE and JW), others are made up of a pair (either IE and EE or IW and EW).

"IE" and "EE," respectively. Similarly, a westward longitudinal shift is often made up of two components: initiating and ending a westward drift, abbreviated "IW" and "EW," respectively.

Although both of the drift periods featured in Figure 1-2 were long in duration when compared to the data's daily sampling rate—lasting approximately 80 and 40 days, respectively—that is not the case for all longitudinal shifts maneuvers. When satellites are observed to change their longitudinal position with shorter drift periods, the beginning and end of the drift may be difficult to discern upon inspection. In these cases, the satellites' longitudinal positions appear to "jump" eastward or westward over time. Fittingly, these types of longitudinal shift maneuvers can be abbreviated "JE" and "JW" for eastward and

westward jumps, respectively.

Table 1.1 describes the six components of longitudinal shift maneuvers discussed along with their abbreviations.

1.2 GEO Satellites Patterns of Life

Satellite patterns of life (PoLs) are descriptions of on-orbit behavior made up of sequences of both natural and non-natural behavioral modes, including routine station-keeping, other on-orbit maneuvers, and uncontrolled motion [10]. After a GEO satellite is inserted into the geostationary belt, its PoL may include any of the six components of longitudinal shift maneuvers described in Table 1.1 separated by periods of station-keeping and natural drift. Although PoLs can take many forms, with various combinations of maneuver components separated by different periods of station-keeping or natural drift, some trends can be observed within the GEO satellite population.

One of the most common PoLs for satellites in GEO is depicted in Figure 1-3. Satellites that adhere to this PoL station-keep at various longitudinal positions, or *stations*, for years on end, and perform infrequent longitudinal shift maneuvers during their operational lifetimes. The satellite featured in Figure 1-3, the European Organization for the Exploitation of Meteorological Satellites' (EUMETSAT) *Meteosat 8* (Satellite ID: 27509), has performed

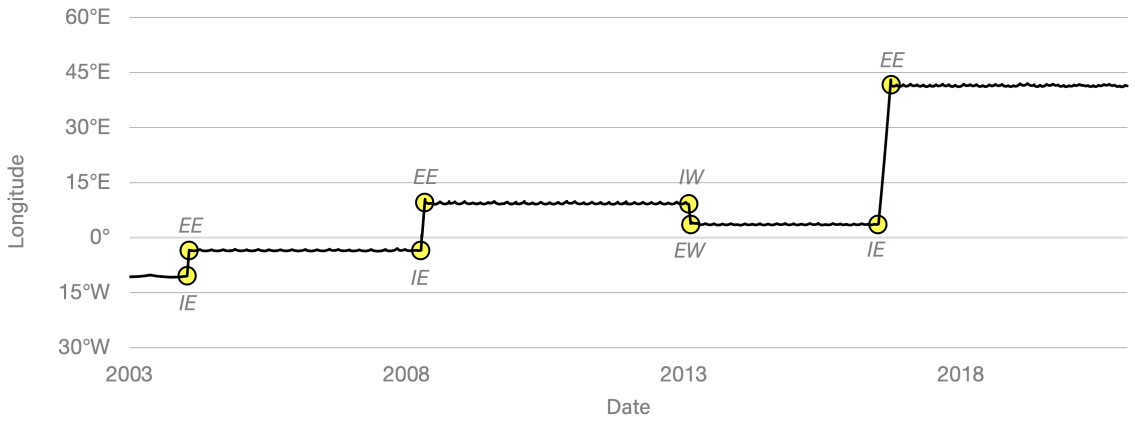

Figure 1-3: The longitudinal position history for EUMETSAT's *Meteosat 8*. This figure shows daily longitudinal positions for EUMETSAT's *Meteosat 8* satellite (Satellite ID: 27509) from January 1, 2003, to December 31, 2020. The satellite was launched on August 28, 2002, and was inserted into the geostationary belt a few weeks later at 10.6°W. Since then, *Meteosat 8* has performed four longitudinal shift maneuvers and occupied five different longitudinal positions. As of January 1, 2021, the satellite is still operational [52]. The plot is annotated with the various maneuver types described in Table 1.1.

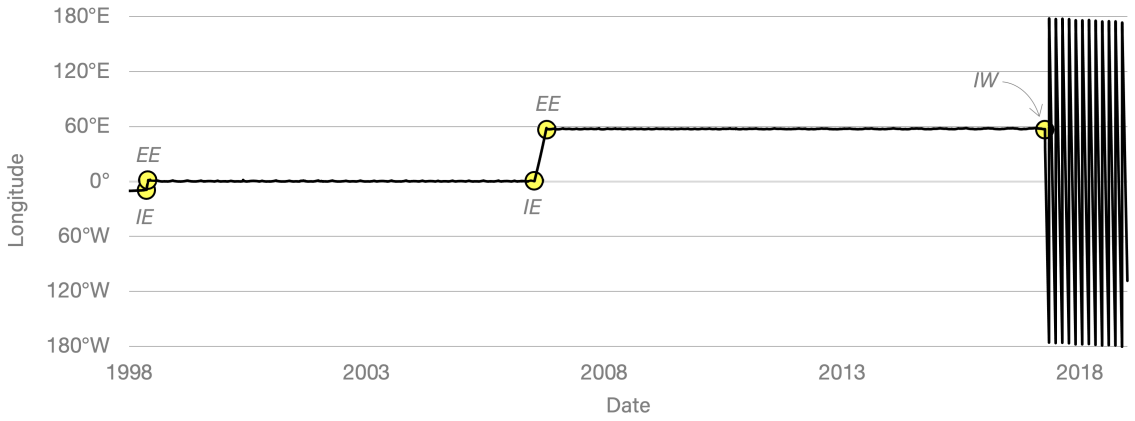

Figure 1-4: The longitudinal position history for EUMETSAT's *Meteosat 7*. This figure shows daily longitudinal positions for EUMETSAT's *Meteosat 7* (Satellite ID: 24932) from January 1, 1998, to December 31, 2018. After its insertion into the geostationary belt in September 1997, *Meteosat 7* performed two longitudinal shift maneuvers and one retirement maneuver. Before it retired, *Meteosat 8* (shown in Figure 1-3) performed a longitudinal shift maneuver to become closer to *Meteosat 7* and limit the coverage gap created by its retirement [30]. The plot is annotated with the various maneuver types described in Table 1.1.

four longitudinal shift maneuvers over its almost two-decade orbital lifetime. Although the four shifts varied in terms of their longitudinal displacement, they shared a common drift rate of approximately 0.5° per day either east or west.

In an attempt to adhere to several U.S. and international guidelines, many satellite operators choose to remove their GEO satellites from the geostationary belt at the end of their operational lifetimes and place them in higher-altitude disposal orbits to reduce the risk of collision with other objects in GEO [25]. Satellites that raise both their apogee and perigee more than 300 km above geostationary orbit are said to have reached a *graveyard orbit* (GYO). Choosing to dispose of a GEO satellite requires a series of maneuvers that can be identified in geographic position time-histories. The unique patterns associated with GEO satellite disposal are a key feature of another common satellite PoL in the geosynchronous region. The satellite featured in Figure 1-4, EUTMETSAT's *Meteosat 7* (Satellite ID: 24932), performed just two longitudinal shift maneuvers in its two-decade orbital lifetime before retiring to GYO in April 2017. After retiring, the satellite's longitudinal position can still be measured over time; the fast drift rate of approximately 7.1° west per day creates the high-frequency saw-tooth pattern seen on the right hand side of Figure 1-4.

Although most satellites in GEO remain operational for many years, others suffer from malfunctions that affect their ability to station-keep or perform longitudinal shift maneu-

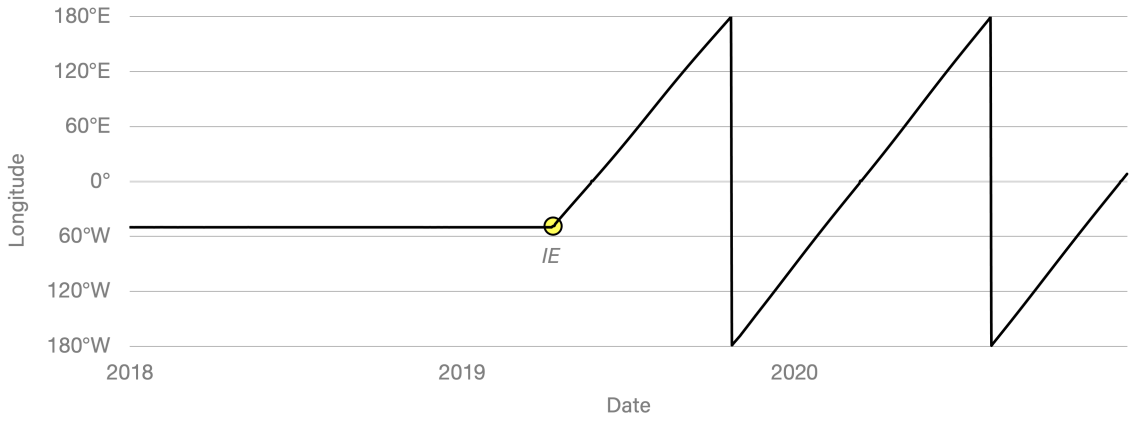

Figure 1-5: The longitudinal position history for Intelsat's *Intelsat 29e*. This figure shows daily longitudinal positions for Intelsat's *Intelsat 29e* (Satellite ID: 41308) from January 1, 2018, to December 31, 2020. On April 7, 2019, the satellite developed a fuel leak, followed soon thereafter by a complete loss of command and control. Since the malfunction, debris has been observed near the satellite that likely originated from the spacecraft itself, which continues to drift eastward in the geostationary belt [19].

vers. In those cases, satellite operators often choose to either abandon their satellites adrift in the geostationary belt or pursue a last-ditch maneuver to place them in a higher-altitude disposal orbit. Figures 1-5 and 1-6 show the longitudinal position histories for two satellites that experienced on-orbit satellite malfunctions. Because malfunctions leave recognizable signatures in GEO satellites' geographic position time-histories, they represent yet another GEO satellite PoL.

Figure 1-5 describes the longitudinal position history for *Intelsat 29e* (Satellite ID: 41308), which suffered a fuel leak on orbit just three years after its launch, causing a disruption in communications services to Intelsat's customers [22]. While attempting to restore the satellite's services, the company reported a second incident, which led to a total loss of communication with the satellite. Days later, *Intelsat 29e* could be observed drifting eastward in the geostationary belt with a drift rate of approximately 1.3° per day, forming a unique, low-frequency saw-tooth pattern as shown on the right hand side of Figure 1-5.

Figure 1-6 describes the longitudinal position history for *VeneSat-1* (Satellite ID: 33414), which also suffered an on-orbit malfunction well before its advertised retirement date. Unlike *Intelsat 29e*, *Venesat-1* appeared to perform two anomalous maneuvers on the same day—March 13, 2020—that sent the satellite drifting westward in an elliptical orbit with both an apogee and perigee above the geostationary belt [21]. With a drift rate of 3.6° west per day, this orbital pattern is distinctly different from that shown on the right hand side of Figure 1-4, which describes a satellite successfully placed in GYO, with both an apogee and

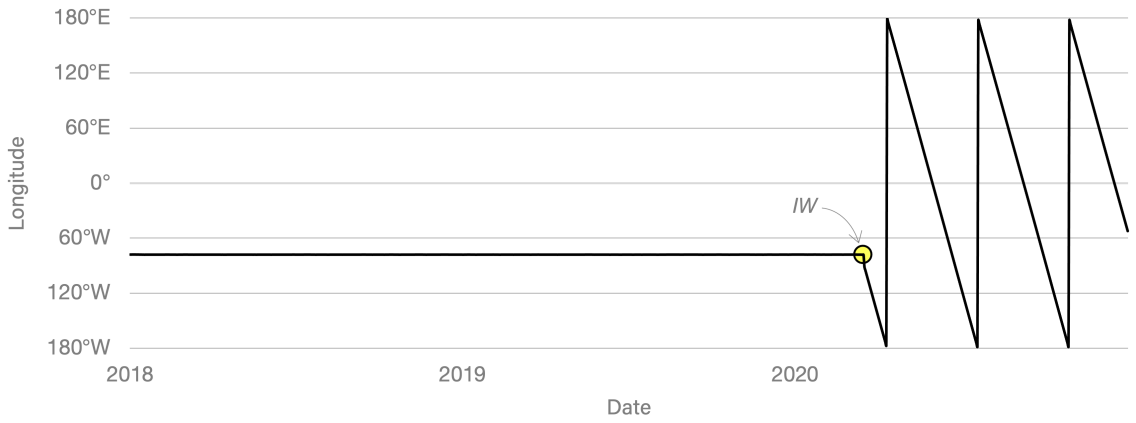

Figure 1-6: The longitudinal position history for Venezuela's *VeneSat-1*. This figure shows daily longitudinal positions for Venezuela's *VeneSat-1* (Satellite ID: 33414) from January 1, 2018, to December 31, 2020. The satellite was launched on October 29, 2008, and was inserted into the geostationary belt a few days later at 77.9°W. *VeneSat-1* pursued consistent station-keeping maneuvers to maintain that station until March 2020, when it suffered an on-orbit malfunction and initiated a westward drift (labeled "IW" in the figure), effectively removing itself from the geostationary belt, but not reaching the graveyard orbit 300 km away.

perigee more than 300 km greater than the geostationary altitude. Although *Venesat-1*'s apogee is greater than this threshold, its perigee is not, resulting in a slower drift rate and a distinct PoL.

In addition to the PoLs highlighted thus far, others feature changes in geographic coordinate positions over time that are *not* due to any of the longitudinal shift maneuver components highlighted in Table 1.1, but rather changes in station-keeping patterns over time, including abandoning station-keeping in the east-west direction, north-south direction, or both. Figure 1-7 shows the longitudinal position history for Russia's *Gorizont 3* (Satellite ID: 11648), an inactive satellite still in GEO. Prior to October 1989, *Gorizont 3* performed east-west station-keeping maneuvers to preserve its longitudinal position approximately once every other month, a notably slower cadence than the satellites featured in Figures 1-3 through 1-6. This station-keeping strategy—which can be seen in the ocean wave-like pattern on the left hand side of Figure 1-7—means the satellite occupied a wider band of longitudinal positions during its operational lifetime, known as a *deadband*. Despite performing none of the longitudinal shift maneuvers described in Table 1.1, the satellite's longitudinal position pattern changed in October 1989, when it abandoned its station and began slowly drifting eastward. Unlike the drift patterns in Figures 1-2 through 1-6, *Gorizont 3*'s drift is clearly non-linear. Due to the asymmetrical distribution of the Earth's mass,

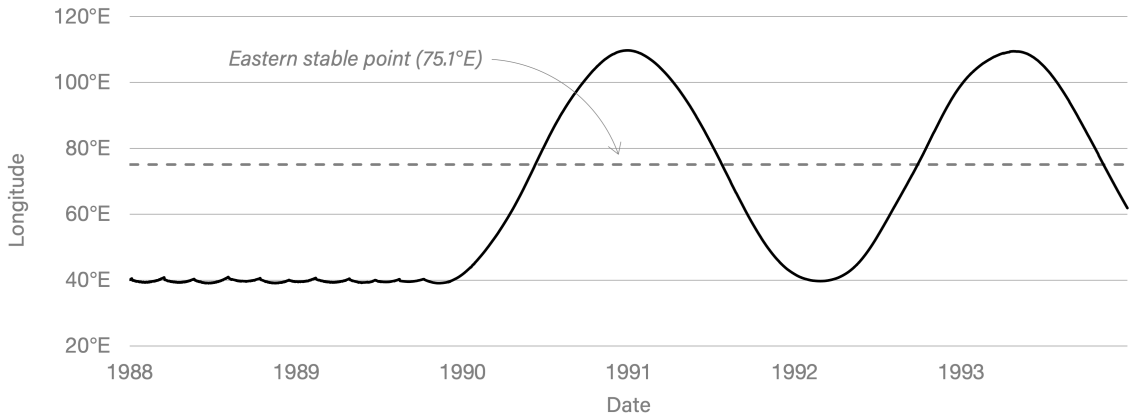

Figure 1-7: The longitudinal position history for Russia's *Gorizont 3*. This figure shows daily longitudinal positions for Russia's *Gorizont 3* (Satellite ID: 11648) from January 1, 1988, to December 31, 1993. In October 1989, the satellite abandoned its station and entered a libration orbit around the eastern stable point, labeled with a dashed line. Although this behavior clearly resulted in a drastic change in longitude, the satellite did not perform any of the components of a longitudinal shift maneuver described in Table 1.1.

satellites in GEO are drawn towards two stable points in the geostationary belt: 75.1°E (known as the *eastern stable point*) and 105.3°W (known as the *western stable point*) [49, 71]. After October 1989, when the satellite abandoned its station-keeping maneuvers, it entered a libration orbit around the eastern stable point, marked with a dashed line in Figure 1-7.

Libration orbits are not uncommon, especially for older satellites in GEO. In 2018, the European Space Agency (ESA) released a report tabulating the number of GEO objects, including debris, in various libration orbits [11]. The report identified 122 objects in libration orbit around the eastern stable point, including *Gorizont 3*, 48 objects in libration orbit around the western stable point, and 19 objects in libration orbit around both stable points.

1.3 Identifying Anomalous Behavior

After a PoL is determined using a satellite's geographic position time-history, it can be used to both predict a satellite's future behavior and classify its recent activities as *nominal* or *anomalous* using more recent data and potential real-time or near-real-time observations [10]. In this work, a satellite's behavior is considered nominal if it adheres to its PoL and anomalous if it deviates from its PoL. Identifying anomalous satellite behavior is of critical

interest to both space situational awareness (SSA) system operators, who may choose to task their sensors to obtain more observations of anomalous behavior, and satellite operators themselves, who may wish to diagnose the root cause of the anomalous behavior being observed.

Consider a GEO satellite with a PoL that resembles that of Figure 1-3. As an observer, one might expect the satellite to continue its pattern of occasionally performing longitudinal shift maneuvers into the future and thus consider additional similar maneuvers to be nominal behavior. However, if upon observing real-time geographic position data, the satellite begins to perform maneuvers much more frequently or more widely varies the length of its drift periods or the speed of its drift rates, such behavior could be considered anomalous and warrant further study.

Now consider a GEO satellite with a PoL more similar to that of Figure 1-4. Since this PoL places the satellite in a high-altitude disposal orbit, a new maneuver of any kind would likely be considered anomalous by most observers. Since satellites in the graveyard orbit are typically drained of propellant and uncontrolled, only a complete lack of maneuvers should be considered nominal. If new data shows the satellite suddenly reducing its drift rate, for example—behavior that clearly indicates the satellite is not defunct—it is almost certainly behaving anomalously.

Deviations from PoLs are also useful for identifying behavior associated with an on-orbit malfunction and satellite retirements. When operational satellites begin a drift period, either with an IE or IW maneuver, but then never perform an EE or EW maneuver soon thereafter, they may be behaving anomalously. If that satellite is relatively new, like *Intelsat 29e* and *VeneSat-1* were during their on-orbit malfunctions, the satellite may be experiencing a similar issue. If the satellite initiates a westward drift, but never ends it, that satellite may be retiring to GYO. In both cases, studying the satellite's other geographic coordinates may offer deeper insight into its behavior.

1.4 Detecting Satellite Maneuvers

In the remaining chapters, a suite of supervised machine learning algorithms for detecting the types of longitudinal shift maneuvers described in Table 1.1 is developed using historical geographic position time-histories from over 1,000 GEO satellites as training data. The algorithms are then tested on more recent geographic time-histories from the 2020 GEO satellite population and the results are applied to PoL anomaly identification.

The following chapter offers both additional background information on the geosyn-

chronous orbital regime and discusses previous research on satellite maneuver detection algorithm development, including several examples that demonstrate the promise of using various supervised and unsupervised machine learning techniques.

The third chapter describes the methodological approach of this work, including how to generate a GEO satellite maneuver database. In this work, GEO satellite geographic position time-histories—like the one plotted in Figure 1-2—are manually labeled with the six types of longitudinal shift maneuvers in Table 1.1 via inspection of the longitude portion of the historical data. Then, the labeled dataset is used to train six maneuver detection algorithms using convolutional neural networks, with one algorithm per maneuver type in Table 1.1. Together, the six algorithms work as a suite to classify longitudinal shift maneuvers.

In the fourth chapter, the suite of algorithms is tested twice on geographic position time-histories for all GEO satellites from January 1 to December 31, 2020, and its performance is discussed. The first test corresponds to a shorter training period, when the suite of algorithms is trained on five years of historical satellite data: geographic position time-histories from January 1, 2015, to December 31, 2019. In the second iteration, the suite is trained on ten years of historical data: geographic position time-histories from January 1, 2010, to December 31, 2019.

In the fifth chapter, the performance of the suite of maneuver detection algorithms, including the precision and recall with which it detects various types of longitudinal shift maneuvers in 2020, are applied to anomaly identification for various GEO satellite PoLs. Several case studies are discussed, including anomalies that could be successfully identified by the suite of satellite maneuver detection algorithms and those that were missed.

The sixth chapter features a brief discussion of how this work interacts with several important issues in space policy and international decision-making in the space domain, including the development of on-orbit norms of behavior and the distribution of spectral and physical space in GEO.

THIS PAGE INTENTIONALLY LEFT BLANK

Chapter 2

Background

This chapter offers background information on the prevalence of longitudinal shift maneuvers in the evolving GEO satellite population as well as a review of the literature surrounding the development of satellite maneuver detection algorithms.

2.1 Evolution of the GEO Satellite Population

Although the first satellite to reach GEO was launched in the 1960s, the concept of syncing a satellite's orbital period with the sidereal day to provide uninterrupted line-of-sight access to observers on the ground was theorized many decades earlier [3]. In his popular 1945 article, "Extra-terrestrial relays," science fiction author Arthur C. Clarke famously described using the concept to support a global communications network with just three equally spaced satellites in geostationary orbit [7]. Earlier references to geosynchronous orbits date as far back as the late 1800s and early 1900s, when Russian scientist Konstantin Eduardovich Tsiolkovsky [51] and Slovene engineer Herman Potočnik [34] published their work on the subject. Over one hundred years later, GEO is now the second most populated orbital regime, with hundreds of operational satellites in orbit [41].

Like the most popular orbital regime—low Earth orbit (LEO), in which satellites orbit the Earth at altitudes of 2,000 km or less—the GEO environment has grown more populated over time. Although the launch of more satellites to GEO has led to more satellites pursuing longitudinal shift maneuvers, satellites that perform longitudinal shift maneuvers remain greatly outnumbered by those that do not. Over the past ten years, from 2011 to 2020, just 5 percent of satellites each year performed at least one longitudinal shift maneuver. Over that same period, only 7.5 percent performed at least one of the components of a longitudinal

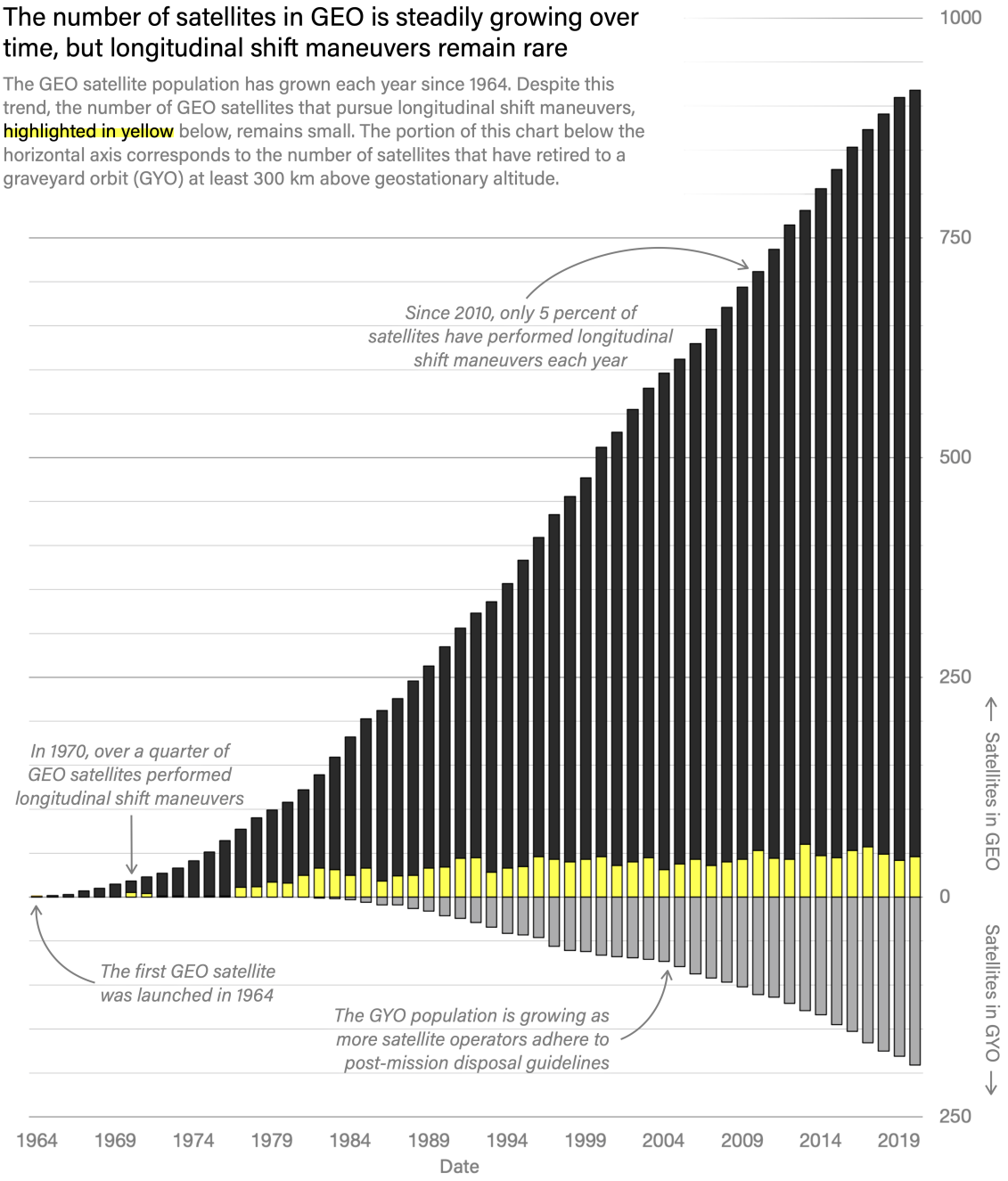

Figure 2-1: Evolution of the GEO satellite population. The portion of this figure above the horizontal axis refers to satellites in GEO, as defined in Section 3.1. Under this definition, the first GEO satellite was NASA's *Syncom 3* (Satellite ID: 858), launched in 1964, as annotated in the figure above. The portion of the figure below the horizontal axis refers to satellites that were once in GEO, but have since spent the majority of a calendar year in a graveyard orbit, at least 300 km above geostationary altitude. The first satellite to meet this definition of the graveyard orbit was U.S. Defense Communications Agency's *OPS 9437* (*DSCS 2-7*) (Satellite ID: 10000). Satellites that performed at least one longitudinal shift maneuver (either a IE-EE or IW-EW pair of maneuvers or a JE or JW maneuver) are highlighted in yellow.

shift maneuver described in Table 1.1, including those associated with retirement to GYO. In general, these figures have decreased over time, since the number of satellites launched to GEO has continued to outpace the number of satellites that perform longitudinal shift maneuvers once they are there.

Figure 2-1 describes the evolution of the GEO satellite population over time. The portion of the bar chart above the horizontal axis represents the number of satellites in GEO each year, while the portion below represents the number of satellites in GYO.[1] The satellites that performed at least one longitudinal shift maneuver in a given year are highlighted in yellow.

Because longitudinal shift maneuvers are relatively rare, the maneuver detection algorithms described in the following chapter are specifically tailored to perform well on imbalanced datasets.

2.2 Previous Research on Satellite Maneuver Detection

Various methods for satellite maneuver detection have previously been developed that vary in their methodology, data input type and source, dependence on machine learning techniques, and effectiveness in various orbital regimes. This section briefly reviews several contributions to the literature, with a focus on the similarities and differences between them and the method described in the following chapter.

One popular strategy for satellite maneuver detection is centered on searching for statistical outliers in space objects' historical orbital element data without depending on machine learning techniques. Kelecy et al. [26] developed a method using smoothed orbital element time-series data generated from historical two-line element sets (TLEs). In their paper, Kelecy et al. segmented the smoothed orbital element time-series data into smaller, user-defined pieces, and fit polynomials to the data included in each segment. They then developed an algorithm that searched the entire smoothed orbital element dataset for relatively large differences between the polynomial fit value at the end of one segment and the beginning of the next. The algorithm used satellites' historical mean motion, semi-major axis and orbital energy to detect in-plane maneuvers and inclination to detect out-of-plane maneuvers. After tuning the algorithm's parameters, it could successfully detect maneuvers in LEO satellite data at small Δv magnitudes on the order of several centimeters-per-second. Patera [38] developed a maneuver detection algorithm with the same premise as Kelecy's,

[1] Satellites "in GEO" are those that meet the requirements described in Section 3.1. Satellites "in GYO" are those that spend the majority of a given year with both their apogee and perigee at least 300 km above geostationary altitude.

but instead used a moving window as opposed to a segmentation strategy. Patera's method used orbital energy data derived from TLEs from the Cheyenne Mountain Operations Center, which could be applied to satellites in any orbital regime.

A second popular strategy for satellite maneuver detection relies on propagating historical orbital parameters and comparing them to subsequent truth data. Relatively large differences between the predicted and actual parameter values are then flagged as maneuvers. This method was applied to maneuver detection in LEO by Lemmens and Krag [29] and Li et al. [31] using TLEs with promising results.

Newer studies apply both supervised and unsupervised machine learning techniques to satellite maneuver detection. Shabarekh et al. [48] presented a method for probabilistically characterizing GEO satellites' PoLs via unsupervised learning and predicting future maneuvers via supervised learning. The method was highly successful at learning and predicting station-keeping maneuvers in GEO, but was not applied specifically to longitudinal shift maneuvers. The study also did not depend on TLE data, but rather synthetic, relatively sparse orbital element data produced by the U.S. Air Force Research Lab. More recently, Bai et al. [2] applied a suite of unsupervised machine learning techniques—including K-means and hierarchical cluster analysis—to historical TLE data and classified orbital maneuvers in LEO by magnitude.

The method described the following chapter was first formulated by Roberts and Linares [45]. The following subsection describes the differences between the methods described in that work and those presented in the following chapter.

2.2.1 Adapting a Previous Framework

Roberts and Linares [45] proposed a novel method for GEO satellite maneuver detection via supervised machine learning using publicly available TLE data. This framework primarily differed from those described earlier in two ways: it relied on historical geographic position data (as opposed to classical orbital elements) and used a convolutional neural network algorithm design.

While the method described in the following chapters also depends on historical geographic position data and convolutional neural networks, it uses a more refined data labeling strategy, and applies the developed algorithms' results to GEO satellite anomaly detection. In the previous study, longitudinal shift maneuvers were labeled in their entirety, without regard to the individual maneuver components described in Table 1.1 of which they are composed. For example, an eastward shift maneuver like the ones described in Figure 1-2 would be labeled as one long longitudinal shift maneuver as opposed to two smaller ones.

In the refined labeling strategy, the same maneuver would be labeled with more detail: the beginning of the eastward drift would be labeled as an IE maneuver, the drift itself would remain unlabeled, and the end of the drift would be labeled as an EE maneuver. The methodology described in the next chapter uses the six longitudinal shift maneuver components described in Table 1.1 to train and test six different satellite maneuver detection algorithms, which together work as a suite for maneuver classification. This method allows for more consistent maneuver labeling and leads to more precise results, as discussed in Chapter 4. Additionally, the suite of maneuver detection algorithms is trained on more historical data, improving its recall when compared to the algorithm evaluated in [45].

THIS PAGE INTENTIONALLY LEFT BLANK

Chapter 3

Methodology

This study is focused on the on-orbit behavior of active satellites in the geosynchronous region. The primary data source for this work is a space object catalog provided by the United States Space Force's (USSF) 18th Space Control Squadron (18 SPCS)—the space control unit responsible for managing the U.S. Space Command's (SPACECOM) SSA program—and made available online to the public at Space-Track.org [53]. In addition to orbital information for active satellites, the SPACECOM catalog includes space objects' historical orbital parameters, which can be used to describe long-term changes in their orbital trajectories over the course of their lifetimes, including the effects of perturbations caused by various natural forces in the near-Earth space environment as well as on-orbit maneuvers designed to preserve or change space objects' orbital characteristics. Historical orbital parameters are described in the catalog using TLEs, which encode space objects' orbits at particular times, known as *epochs*. A collection of TLEs, ordered by epoch, is known as a *TLE time-history* [26]. Figure 3-1 shows an annotated TLE time-history for *GOES-4* (Satellite ID: 11964), a satellite that was a part of the U.S. National Oceanic and Atmospheric Administration's (NOAA) Geostationary Operational Environmental Satellite (GOES) system, as an example.

3.1 Defining the GEO Region and Identifying GEO Satellites

Although the SPACECOM catalog includes various types of space objects—such as payloads, rocket bodies, and debris—this analysis focuses only on the behavior of active satel-

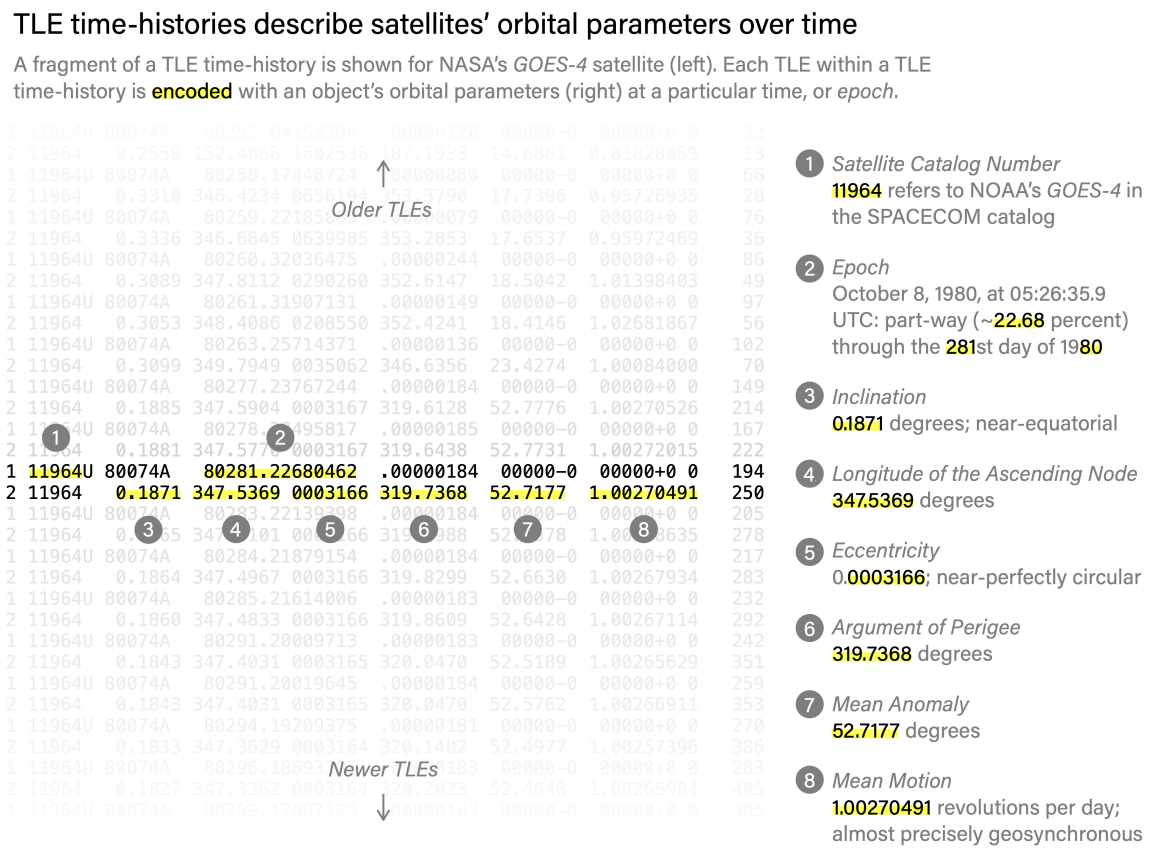

Figure 3-1: Annotated TLE time-history for NOAA's *GOES-4*. This figure shows a portion of NOAA's *GOES-4*'s (Satellite ID: 11964) TLE time-history (left). The encoded orbital parameters described in one particular TLE (right) show that the satellite is almost precisely in geostationary orbit. This TLE time-history was reproduced on CelesTrak.com, not queried from the password-protected Space-Track.org database [5].

lites, and thus only references data for payload objects.[1] Similarly, the catalog also includes objects in various orbital regimes, such as LEO, medium Earth orbit (MEO), GEO, and regimes associated with non-Earth central bodies like the Sun and Moon. Since this study is focused on the geosynchronous region, only payload objects that were determined to be in GEO at least once before the end of the study period on December 31, 2020, are referenced. In this case, a geosynchronous orbit is defined as any orbit that is fully enclosed in the geosynchronous region as described by the Inter-Agency Space Debris Coordination Committee (IADC) [23]. By this definition, GEO orbits have both an apogee and perigee altitude within 200 km of geostationary altitude and an inclination between -15 and 15 degrees. Although some objects may pass through the geosynchronous region during their orbital periods, this definition for GEO only includes objects that are in this region for their entire orbital period.

To determine whether an individual TLE places its corresponding object in GEO using the IADC's definition, a portion of the TLE's encoded orbital elements must be converted into apogee and perigee altitudes (h_a and h_p, measured in meters above the Earth's surface) using the following formulas:

$$h_a = \sqrt[3]{\frac{G \times M_\oplus}{(n \times \frac{2\pi}{86400})^2}}(1+e) - R_\oplus \tag{3.1}$$

$$h_p = \sqrt[3]{\frac{G \times M_\oplus}{(n \times \frac{2\pi}{86400})^2}}(1-e) - R_\oplus \tag{3.2}$$

where G is the gravitational constant ($\approx 6.674 \times 10^{-11}$ $\mathrm{m^3 kg^{-1} s^{-2}}$), $M_\oplus$ is the is the mass of the Earth ($\approx 5.972 \times 10^{24}$ kg), $R_\oplus$ is the radius of the Earth ($\approx 6.371 \times 10^6$ m), n is the TLE-encoded mean motion (in revolutions per day), and e is the unitless TLE-encoded eccentricity.

After performing this calculation on the TLEs for all payload objects available in the SPACECOM catalog and adhering to the data cleaning practices described in Section C.2, it can be determined that there have been 1,109 satellites in GEO for at least one day during the study period.[2]

[1] Objects that were uncategorized in the catalog on the date it was accessed (February 1, 2021), were also included in this study, since those objects may be re-labeled as payloads once they are categorized by 18 SPCS.

[2] This figure can be seen as the sum of the satellites above and below the horizontal axis in the 2020 portion of Figure 2-1.

3.2 Preparing a Dataset for Training and Testing

The data encoded in a TLE time-history must be transformed into geographic coordinates, labeled with the various maneuver types described in Table 1.1, and written in a format that can be used to train and test the satellite maneuver detection algorithms. The following subsections describe the steps required to convert TLE time-histories from the publicly available SPACECOM catalog into labeled *geographic time-history segments*, the required data format for training and testing the various maneuver detection algorithms.

3.2.1 Converting TLE Time-histories to Geographic Coordinates

The geographic coordinate data presented in Figure 1-2, also known as a *geographic time-history*, is evenly spaced in time. TLE time-histories, however—which are used to derive geographic time-histories—are not evenly spaced in time. The epochs encoded in each TLE time-history are more densely spaced for some satellites and more sparsely spaced for others. To convert unevenly spaced TLE time-histories to evenly spaced geographic time-histories, an appropriate time step must first be selected at which to sample the TLE time-histories.

To inform the selection of the geographic time-histories' time step, consider the average separation between epochs for GEO satellites, also known as the *average age of TLEs*. The average age of TLEs at various positions across the geostationary belt over time is shown in Figure 3-2. In the 1990s, TLE epochs were typically separated by about 2 to 6 days. TLE time-histories associated with satellites in the western hemisphere, from 180°W to 0° in Figure 3-2, featured smaller TLE separations than satellites in the eastern hemisphere. In the 2000s, the average age of TLEs for GEO satellites was shorter—approximately 2 to 4 days—with less variation across the two hemispheres. In the 2010s, the average age for GEO satellites' TLEs fell to approximately 1 day for all longitudinal positions. Thus, a one-day time step is an appropriate choice for this study.

At each time step in a satellite's geographic time-history, one TLE must be selected from the satellite's TLE time-history with which to calculate the satellite's geographic position. The appropriate TLE can be found by searching the satellite's TLE time-history and identifying the TLE with an epoch closest to a given time step in the geographic time-history, known as the *nearest TLE*. For example, the nearest TLE with which to calculate *GOES-4*'s geographic position on October 8, 1980, is the TLE highlighted in yellow in Figure 3-1. This same TLE is also the nearest TLE for the next day in the satellite's geographic time-history, October 9. On the following day, however, October 10, the nearest TLE is the next one in the satellite's TLE time-history—the pair of lines below the ones

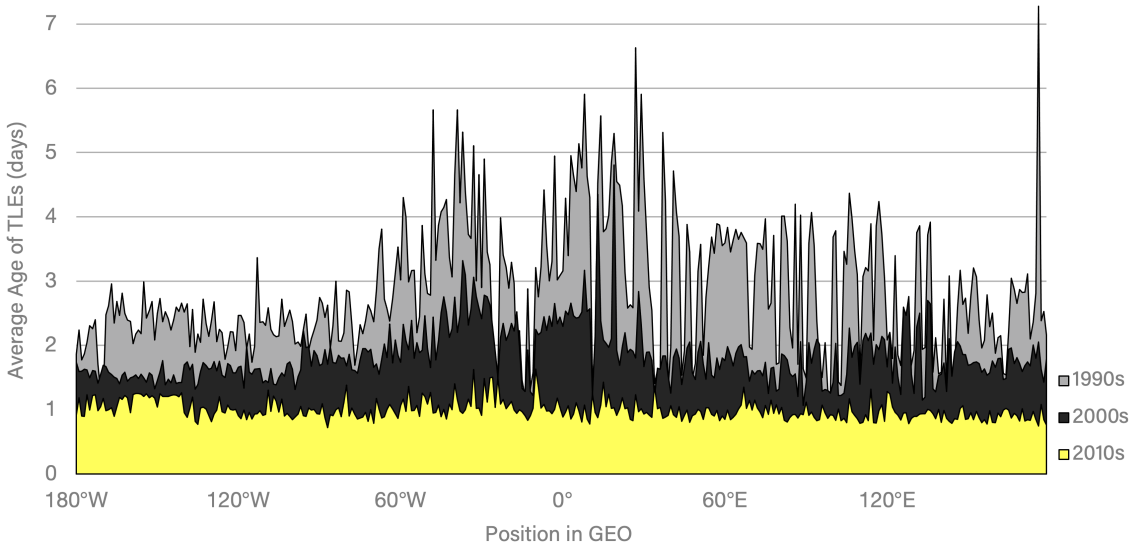

Figure 3-2: Average age of TLEs in the 1990s, 2000s, and 2010s for GEO satellites by longitudinal position. In general, the average age of TLEs has decreased over time. In earlier decades, the average age of TLEs varied with longitude. In the 1990s, for example, TLEs for satellites near 100°W (an ideal position for offering coverage to the continental United States) were published approximately once every two days, whereas TLEs for satellites near 25°E (an ideal position for offering coverage to central Africa and eastern Europe) were published only once every four to six days. More recently, however, in the 2010s, TLEs satellites at all longitudinal positions are published on average once per day.

highlighted in yellow, since that newer TLE's epoch is closer in time to October 10 at midnight.

If the nearest TLE's epoch is earlier than a given time step in a satellite's geographic time-history, the TLE must be propagated forward to the date and time associated with the given time step. Similarly, if the nearest TLE's epoch is later than the given time step, the TLE must be propagated backwards in time. Since TLEs lose accuracy with time, TLEs should not be propagated forward or backwards by more than two weeks. If the nearest TLE's epoch is more than two weeks away from a given time step, no geographic position should be calculated for that time step. This study uses the SGP4/SDP4 model [55] included in the PyEphem Python library for propagation [40]. The propagated TLE, known as the *time-adjusted nearest TLE*, can then be saved as a PyEphem Object.

At each time step, the orbital parameters encoded in the time-adjusted nearest TLE can be converted into geographic coordinates—latitude, longitude, and altitude—algorithmically using a coordinate system transformation [54, 172]. This study uses the PyEphem Object's built-in "sublat," "sublong," and "elevation" properties to compute the geographic positions

directly from the time-adjusted nearest TLE.

Recall from the previous subsection that not all 1,109 GEO satellites included in this study necessarily spend the entire study period within the geosynchronous region. Although all of the GEO satellites spend at least one day in the GEO region according to Section 3.1's definition of a GEO satellite, they each spend a portion of their operational lifetime below GEO (in the days after they are launched, but before they reach GEO) and many of them leave GEO once reaching it (perhaps due to a longitudinal shit maneuver, an on-orbit malfunction, retirement to GYO, or abandoning station-keeping). To record whether each object falls within the GEO region at each time step in the study period, a new binary field called "GEO Status" can be included in the geographic position time-history as a fourth feature after geographic latitude, longitude, and altitude.

Since this study is focused on satellite behavior in GEO (as opposed to anything that happens before the satellite reaches GEO), the geographic time-histories should be truncated such that the first time step in the time-history corresponds to the first day in which the satellite falls within the GEO region.

3.2.2 Labeling Longitudinal Shift Maneuvers

The longitude portion of geographic time-histories can be plotted, as shown in Figures 1-3 through 1-7, and the six types of longitudinal shift maneuvers featured in Table 1.1 can be labeled by inspection. In addition to labeling any time steps on which maneuvers occur, a number of time steps before and after maneuvers should also be labeled. These extra time steps are known as the *maneuver buffer period* (b). Including a maneuver buffer period of any size will assist the convolutional neural network described later in this chapter in recognizing the various maneuver types, as maneuver patterns are most recognizable when observed alongside geographic position data from before and after the day the maneuver occurs. Figure 3-2 shows an example of manually labeled longitudinal position data with a buffer period of 3 days.

If a drift period is too short to accommodate the buffer periods associated with a IE-EE or IW-EW pair of maneuvers—that is, its length is less than or equal to $2b + 1$ days—then that drift period should be labeled JE or JW, respectively, with a buffer period labeled both before and after.

Under the described labeling strategy, an individual day should only be labeled with one of the six longitudinal shift maneuver types described in Table 1.1, but consecutive days may be labeled with two different types. Additionally, any individual maneuver type should appear on no fewer than $2b + 1$ consecutive days, as shown in Figure 3-3.

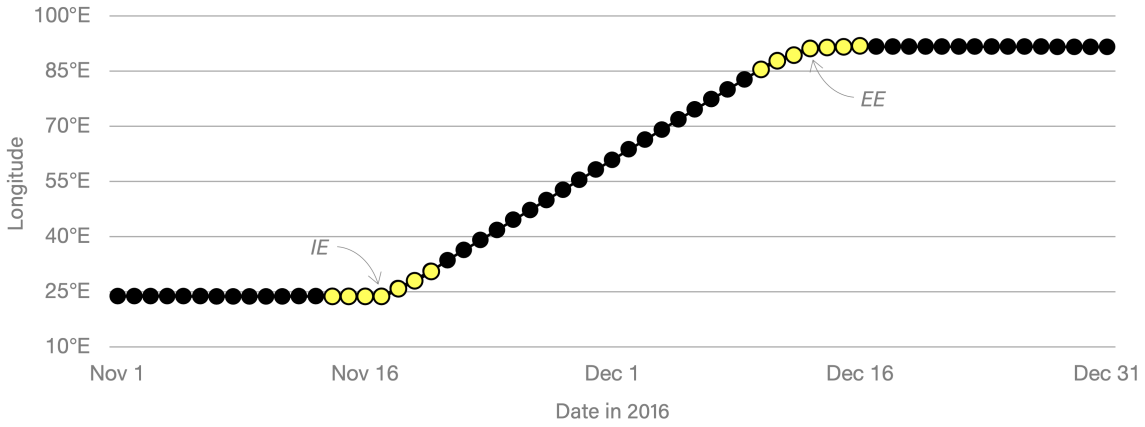

Figure 3-3: An example of the labeling process for two types of longitudinal shift maneuvers. This figure shows daily longitudinal positions for Telesat's *Nimiq 2* from November 1 to December 31, 2016. Two components of a longitudinal shift maneuver are labeled in this plot with a maneuver buffer period of 3 days. This particular buffer period ensures that each maneuver is labeled across a cluster of at least 7 days.

3.2.3 Segmenting the Geographic Time-histories

Since the GEO satellites included as part of this study entered the GEO region at different times, their geographic position time-histories vary in length. Those that entered GEO at the tail end of the study period might have only several days of geographic position data. Others may have spent decades in the GEO region, and therefore have much longer geographic time-histories. In order to create a dataset on which to train the maneuver detection algorithms to identify the various maneuver types, each geographic time-history—regardless of its length—should be divided into segments and each segment labeled with the types of maneuvers it contains, if any.

To segment the geographic time-histories, a frame width (f) and step size (s) should be selected, such that the segments are each $f+1$ days long and their start dates are separated by s days. The first segment created under a segmentation strategy with a frame width of 28 and a step size of 14, for example, would begin on January 1 and end on January 29, while the second segment would begin on January 15 and end on February 12. Notice that when $s \leqslant f$, individual days appear in more than one segment. In the same example when $f = 28$ and $s = 14$, each date appears in two different segments, which will later offer the detection algorithms two opportunities to detect maneuvers on each day.

After the segments are created, they must be labeled based on whether any of the maneuver types from Table 1.1 appear during that period. Since maneuver types are most

recognizable when they are preceded and followed by a buffer period, only segments that contain both maneuvers and their corresponding buffer periods in their entirety should be labeled as such. That is, a segment should be labeled with a maneuver type if it contains no fewer than $2b + 1$ individual days with a particular maneuver label. To develop a training dataset for the maneuver detection algorithms described in the next section, the frame width, step size, and maneuver buffer period should be selected such that $f \geqslant s$ and $s > 2b + 1$. These considerations increase the number of opportunities the maneuver detection algorithms have to detect maneuvers and ensure that at least some segments contain labeled maneuvers.

Note that under the described labeling strategy, an individual segment may be labeled with more than one of the maneuver types described in Table 1.1.

3.2.4 Preprocessing the Geographic Time-history Segments

Prior to training the maneuver detection algorithms, the geographic time-history segments should be preprocessed to account for two peculiarities of the longitudinal measurement system.

The geographic time-history segments, like the geographic time-histories themselves, measure longitude on a scale of -180 (corresponding to 180°W in the geostationary belt) to 180 degrees (corresponding to 180°E), as shown in Figures 1-2 through 1-7. Despite this convention, there is no physical significance of the 180th meridian in this measurement system. When a satellite traverses the 180th meridian, however—meaning it crosses from 179.9°E to 179.9°W, or vice versa, due to a longitudinal shift maneuver or as part of the satellite's natural drift—it may appear to an untrained observer like a discontinuity on the longitudinal position plot. To account for this issue, geographic time-history segments that include 180th meridian crossings should have their longitudinal scales adjusted. For example, if a satellite begins a segment with a longitudinal position of 175°E, then initiates and ends an eastward drift such that it ends the segment with a longitudinal position of 175°W, that segment's longitudinal scale should be adjusted: instead of ranging from -180 to 180 degrees, it should range from -180 to 540 degrees, and all western hemisphere measurements should be increased by 360 degrees. Such a change would make the example segment appear to begin at a longitude reading of 175 degrees and end at 185 degrees, with no observable discontinuity at the 180th meridian.

In addition, the geographic time-history segments should be normalized such that their minimum and maximum longitudinal measurements are mapped to 0 and 1 respectively. This process allows the maneuver detection algorithms to be trained to detect maneuvers

regardless of their starting and ending positions on the longitudinal scale and the drift rate associated with any shift maneuvers.

3.2.5 Resampling the Training Dataset

In order to measure the success of the maneuver detection algorithms designed in the following section, a portion of the geographic time-history segments must be reserved and not used for training. For this study, all segments that contain a date in the year 2020 are reserved for this purpose, and are known as the *test dataset*. All other segments, which form the *train dataset* will be used to train the algorithms.

Since the six maneuvers described in Table 1.1 are relatively rare, the vast majority of the geographic time-history segments used for training contain no maneuvers of any kind. To obtain a more balanced training dataset—where the number of segments that contain maneuvers (known as the *positive class*) is closer to the number that contain no maneuvers (known as the *negative class*)—resampling strategies should be used on the train dataset to balance the two classes [4]. When used in combination, over-sampling the positive class (using methods such as SMOTE [6] or ADASYN [17]) and under-sampling the negative class (by simply removing a portion of the segments that contain no maneuvers) have been measured to perform particularly well [18].

3.3 Algorithm Design

Six one-dimensional convolutional neural networks (CNNs) can be trained to identify each of the six types of longitudinal shift maneuvers described in Table 1.1 using the Keras Python library [12]. This subsection describes the parameters that were selected to create and segment all GEO satellites' geographic time-histories and form the dataset needed to train the CNN-based algorithms. It also includes a description of the parameters selected to develop preliminary versions of the algorithms for each of the maneuver types that are evaluated in the following chapter.

Note that the following selections represent an initial design for a suite of maneuver detection algorithms, not the result of a hyperparameter optimization process. Future studies would likely benefit from tuning the hyperparameters, which may lead to improvements in precision and recall when compared to the results presented in the following chapter.

3.3.1 Labeling, Segmentation, and Resampling

The algorithms evaluated in the following chapter depend on geographic time-histories labeled using the labeling strategy described in the previous section. To create the geographic time-history segments, maneuvers were labeled with a 3-day maneuver buffer period ($b = 3$). Such a selection ensures that each maneuver is labeled within a cluster of at least 7 days, as shown in Figure 3-3. After the geographic time-histories were labeled, they were divided into segments of length 28, with a 1-day separation between the start dates of the segments ($f = 28$; $s = 1$). These selections ensure that each day within a GEO satellite's geographic time-history appears in 29 different segments, offering the algorithms many opportunities to identify maneuvers on each day.

After the geographic time-history segments were created, the positive class within the training dataset was over-sampled using the ADASYN method with a 0.75 sampling strategy and the negative class was randomly undersampled with a 0.80 sampling strategy.

3.3.2 Choosing Parameters for the Convolutional Neural Network

This re-sampled training data was then used to fit a CNN model with the following layers:

1. A one-dimensional CNN layer (created using Keras' "Conv1D" class) with 32 filters, a kernel size of 3, and the rectified linear unit (ReLU) activation function;
2. A second one-dimensional CNN layer with the same parameters as the first layer;
3. A dropout layer (created using Keras' "Dropout" class) with a frequency of 0.5;
4. A one-dimensional max pooling layer (created using Keras' "MaxPooling1D" class) with a pooling size of 2;
5. A dense layer (created using Keras' "Dense" class) with a size of 100 and the ReLU activation function; and
6. A second dense layer with the "Softmax" activation function, sized to the number of geographic time-history segments included in the training dataset.

3.3.3 Training the Algorithm

In the following chapter, each of the six maneuver detection algorithms designed in this section are evaluated twice: once after being trained on five years' worth of geographic time-history segments (corresponding to dates between January 1, 2015, and December 31,

2019) and once after being trained on ten year's worth of data (corresponding to dates between January 1, 2010, and December 31, 2019). In both cases, the algorithms are tested against geographic time-history segments from January 1 to December 31, 2020.

THIS PAGE INTENTIONALLY LEFT BLANK

Chapter 4

Results

The algorithms described in the previous chapter can be used to detect each of the six satellite maneuver types using any GEO satellite's geographic position data that is segmented using the same segmentation strategy as the training dataset. This chapter evaluates the geographic time-histories segments for all satellites in GEO in 2020.

With a frame width of 28 days, a step size of 1 day, and hundreds of operational GEO satellites in orbit, there are more than 400,000 segments in this test period. Like previous years, the six maneuver types described in Table 1.1 were not equally common in 2020. Figure 4-1 describes the number of segments labeled with each of the six maneuver types for that year. Note that in general, the number of segments that contain maneuvers in a particular training or testing dataset is not necessarily equal to the total number of maneuvers actually performed by GEO satellites during that time. For this particular labeling and segmentation strategy, one maneuver is captured in many different segments and thus the number of segments labeled with each maneuver type in Figure 4-1 is much greater than the number of maneuvers actually pursued in 2020.

Although the rarest maneuver type (JW) and the most common maneuver type (IW) differ by more than an order of magnitude, it should be noted that for each maneuver type, the vast majority of the segments in 2020—over 99.6 percent in each case—do not contain maneuvers.

4.1 Performance Evaluation Metrics

The following two sections describe the performance of each algorithm via the distribution of the four components of a traditional binary confusion matrix [27, 254]:

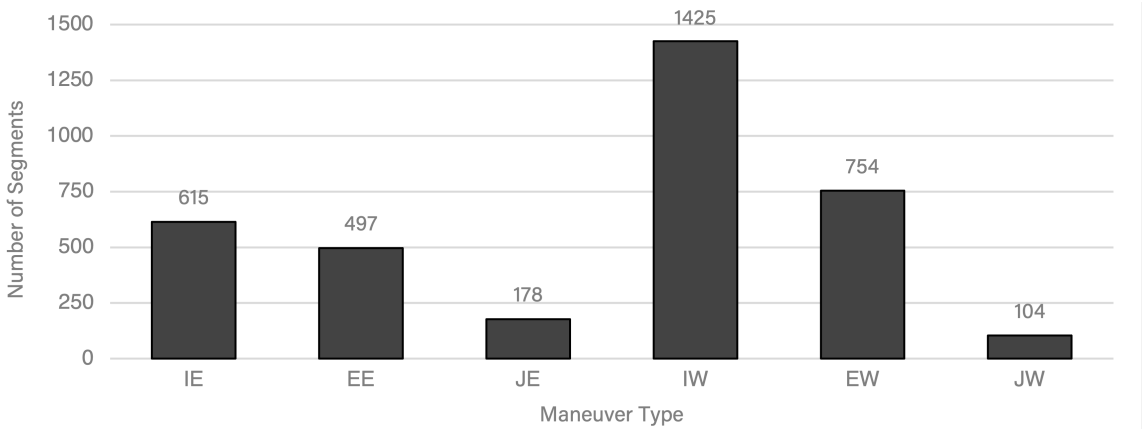

Figure 4-1: Distribution of the six maneuver types in 2020. This figure compares the number of segments in the test dataset that are labeled with each of the six maneuver types described in Table 1.1.

1. "True positive" (TP) outcomes are those in which the algorithms detect a maneuver that did indeed occur in a particular segment [50];

2. "False positive" (FP) outcomes are those in which the algorithms detect a maneuver that actually did not occur in a particular segment (also known as a Type I error);

3. "False negative" (FN) outcomes are those in which the algorithms fail to detect a maneuver that really did occur in a particular segment (also known as a Type II error); and

4. "True negative" (TN) outcomes are those in which the algorithms do not detect a maneuver in one of the many segments in which a maneuver did not occur.

The true positive and false negative outcomes for a particular maneuver type make up the positive class (P) and sum to the total number of segments that actually contain that type of maneuver:

$$P = TP + FN \tag{4.1}$$

The true negative and false positive outcomes for a particular maneuver type make up the negative class (N) and sum to the total number of segments that do not contain that type of maneuver:

$$N = TN + FP \tag{4.2}$$

The four components of the confusion matrix are useful for calculating critical metrics that can be used to evaluate the algorithms' performance, including *accuracy*, *recall*, and

precision. The accuracy of a maneuver detection algorithm is an expression of how often it correctly identifies behavior across both the positive and negative classes:

$$Accuracy = \frac{TP + TN}{P + N} = \frac{TP + TN}{TP + FN + TN + FP} \tag{4.3}$$

Since the vast majority of the geographic time-history segments in the test dataset are in the negative class, this metric is not particularly useful for understanding the algorithms' overall performance; other performance metrics may be more revealing. The recall of a maneuver detection algorithm is simply the fraction of the positive class that is correctly identified by the algorithm (i.e. the number of maneuvers detected):

$$Recall = \frac{TP}{P} = \frac{TP}{TP + FN} \tag{4.4}$$

The precision of a maneuver detection algorithm describes the fraction of the segments the algorithm identified as containing a maneuver that actually do contain one:

$$Precision = \frac{TP}{TP + FP} \tag{4.5}$$

Lastly, the F_1 score is the harmonic mean of the recall and precision:

$$F_1 = \frac{2 \times TP}{2 \times TP + FP + FN} \tag{4.6}$$

In addition to presenting the four components of the confusion matrix for each algorithm, the following two sections also include the algorithms' accuracy, recall, precision and F_1 scores.

4.2 Results With a 5-Year Training Dataset

Table 4.1 describes the four components of the confusion matrix for each of the six satellite maneuver detection algorithms after they were trained on five years' worth of GEO satellites' geographic time-history segments. The last four columns of the table present the results of the performance metrics calculations described in the previous subsection.

Figure 4-2 presents the same data as Table 4.1, but grouped by class, for clarity.

Five of the six maneuver types—including the four that occurred most in 2020—exhibited recall rates 65 percent or more. For two of the six types, those associated with ending a longitudinal drift, the recall was much higher: over 90 percent of the positive class was

	TP	FP	FN	TN	Accuracy	Recall	Precision	F_1 Score
IE	400	327	215	399,608	99.9%	65.0%	55.0%	59.6%
EE	451	1,313	46	398,740	99.7%	90.7%	25.6%	39.9%
JE	49	300	129	400,072	99.9%	27.5%	14.0%	18.6%
IW	1,259	1,920	166	397,205	99.5%	88.4%	39.6%	54.7%
EW	684	804	70	398,992	99.8%	90.7%	46.0%	61.0%
JW	79	576	25	399,870	99.8%	76.0%	12.1%	20.8%

Table 4.1: Performance metrics for the suite of satellite maneuver detection algorithms on a segment-by-segment basis after training on five years' worth of GEO satellite data. The last four columns of this table present the performance metrics of the six maneuver detection algorithms after they were trained on five year's worth of GEO satellite data (geographic time-history segments containing dates between January 1, 2015, and December 31, 2019) and evaluated on the GEO satellite population in 2020.

identified. All six of the algorithms, however, exhibited poor precision; false positives often outnumbered true positives. Since the F_1 scores weigh both recall and precision, they too were poor: only half of the algorithms have an F_1 score over 50 percent.

Although Table 4.1 and Figure 4-2 provide a detailed view of the algorithm suite's performance on a segment-by-segment basis, satellite operators and SSA analysts may be more interested in its performance on a maneuver-by-maneuver basis. Recall that each maneuver that actually occurred in 2020 is captured in more than one segment. A maneuver that is labeled over 7 days, for example, like the two shown in Figure 3-3, appears fully in 23 different segments in this segmentation strategy. Instead of reporting the results of the algorithm on each of those 23 segments, consider their performance as a group.

Figure 4-3 uses this concept to plot the suite of maneuver detection algorithm's performance on a maneuver-by-maneuver basis. Each row in the figure corresponds to a satellite that actually performed at least one type of longitudinal shift maneuver in 2020 and is labeled with the satellite's SPACECOM Satellite ID number. Each square represents a satellite's behavior for one week in 2020. Those outlined in black contain a maneuver—that is, four of the seven days in that week were *labeled* with one of the six different maneuver types. Squares in which any of the six algorithms identified a maneuver—that is, at least four days in that week were *predicted* to contain maneuvers (meaning those days' 23 segments were each flagged as containing a maneuver)—are highlighted in yellow.

The confusion matrix under this maneuver-by-maneuver formulation is more favorable

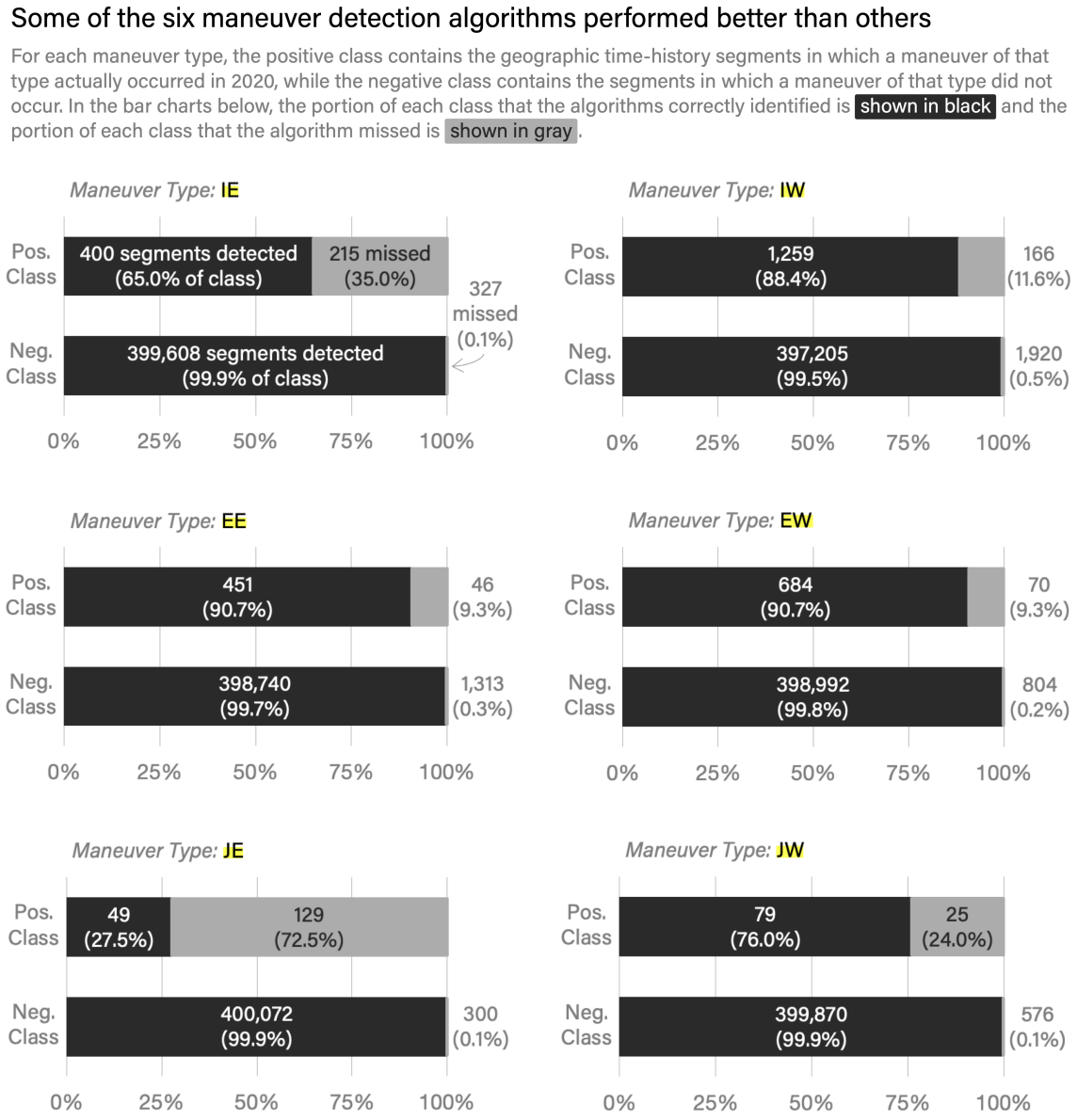

Figure 4-2: Performance metrics for the suite of satellite maneuver detection algorithms on a segment-by-segment basis after training on five years' worth of GEO satellite data. The true positive and false negative portions of the confusion matrices are shown in the positive class of each bar chart in black and gray, respectively. The true negative and false positive portions of the confusion matrices are shown in the negative class of each bar chart in black and gray, respectively.

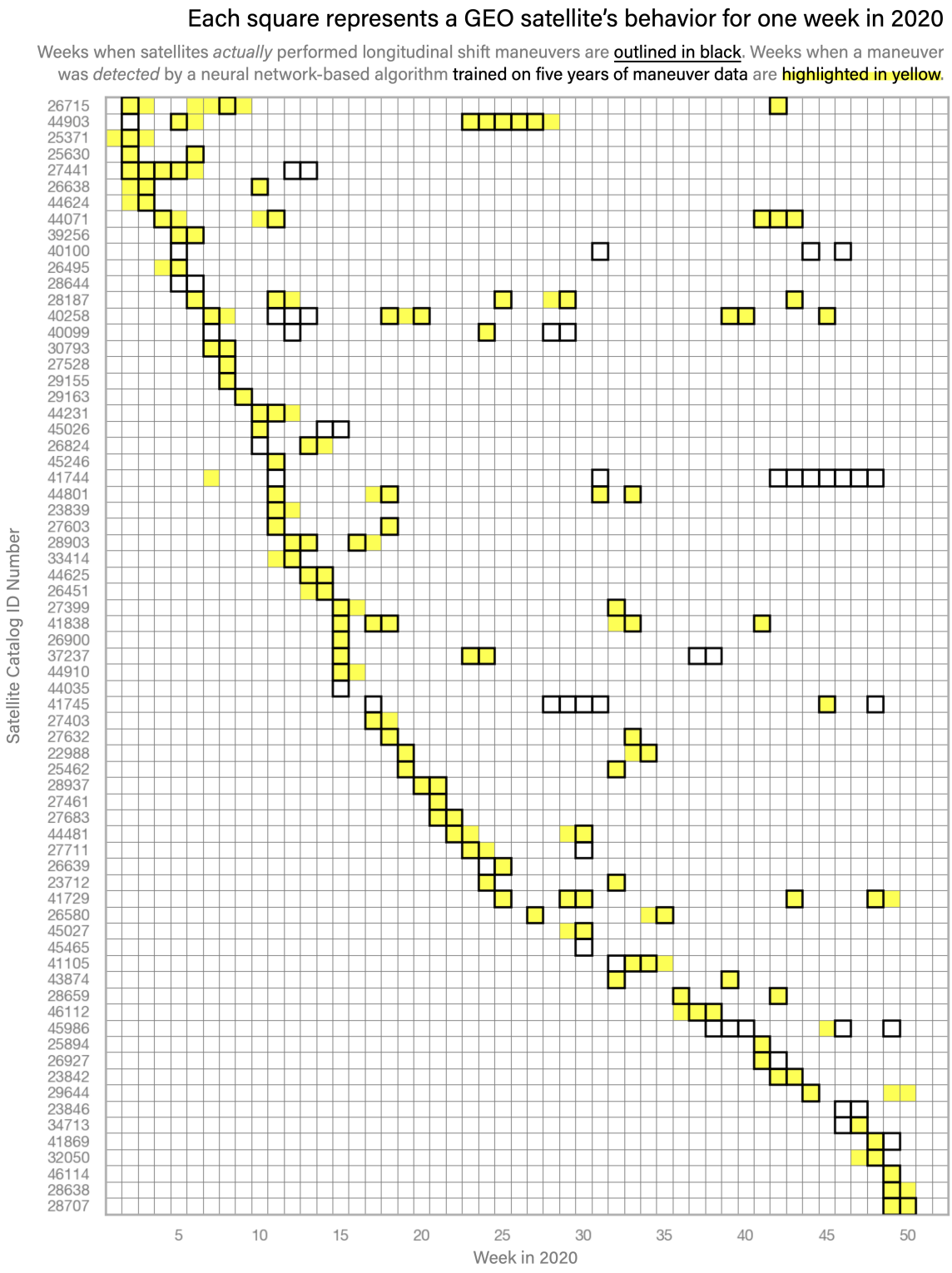

Figure 4-3: Detection results for the suite of satellite maneuver detection algorithms on a maneuver-by-maneuver basis after training on five years' worth of GEO satellite data. The rows of the figure correspond to the 71 GEO satellites that performed a longitudinal shift maneuver of any kind in 2020 ordered by the week of their first maneuver.

than that of the segment-by-segment formulation for each maneuver type presented earlier in this section. With 1,104 satellites in the test dataset in 2020 and 52 weeks per year there are 57,408 total outcomes in the confusion matrix, with 173 in the positive class and 57,235 in the negative class and the following distribution:

1. 122 true positives;
2. 47 false positives;
3. 51 false negatives; and
4. 57,188 true negatives.

This confusion matrix corresponds to an accuracy of 99.8 percent, recall of 70.5 percent, precision of 72.2 percent, and an F_1 score of 71.3 percent.

4.3 Results With a 10-Year Training Dataset

When the same algorithms are trained on ten year's worth of GEO satellite data—meaning the training dataset included geographic time-history segments with dates between January 1, 2010, and December 31, 2019—instead of five, they demonstrate improved performance, in general. Table 4.2 describes the four components of the confusion matrix for all six maneuver detection algorithms when evaluated on the same 2020 test data.

Five of the six maneuver algorithms achieved higher recall than they did in the previous subsection, with algorithms associated with the two least common maneuver types (JE and JW) showing the most improvement. Interestingly, the precision and F_1 score metrics in Table 4.2 are only better for two of the six algorithms and poorer for the other four. Like Figure 4-2, Figure 4-4 shows the components of the confusion matrices grouped by class.

Like the case with five years of training data, the confusion matrix for this iteration of the algorithm suite under the maneuver-by-maneuver formulation introduced in the previous section is more favorable than that of the segment-by-segment formulation for each maneuver type:

1. 122 true positives;
2. 47 false positives;
3. 51 false negatives; and
4. 57,188 true negatives.

	TP	FP	FN	TN	Accuracy		Recall		Precision		F_1 Score	
IE	400	983	215	398,952	99.7%	↓0.2	65.0%	–	28.9%	↓26.1	40.0%	↓19.6
EE	454	2,057	43	397,996	99.5%	↓0.2	91.3%	↑0.6	18.1%	↓7.5	30.2%	↓9.7
JE	115	592	63	399,780	99.8%	↓0.1	64.6%	↑37.1	16.3%	↑2.2	26.0%	↑7.4
IW	1,277	1,230	148	397,895	99.7%	↑0.2	89.6%	↑1.3	50.9%	↑11.3	65.0%	↑10.3
EW	691	1,208	63	398,588	99.7%	↓0.1	91.6%	↑0.9	36.4%	↓9.6	52.1%	↓8.9
JW	102	772	2	399,674	99.8%	–	98.1%	↑22.1	11.7%	↓0.4	20.9%	↑0.1

Table 4.2: Performance metrics for the suite of satellite maneuver detection algorithms on a segment-by-segment basis after training on ten years' worth GEO satellite data. The last eight columns of this table describe the performance metrics of the six maneuver detection algorithms after they were trained on ten year's worth of satellite data and evaluated on the GEO satellite population in 2020. The differences between the performance metrics in this table and those in Table 4.1 are shown with ↑ and ↓ symbols representing score increases and decreases, respectively.

The results of the maneuver-by-maneuver formulation evaluation are shown in Figure 4-5.

When compared to the results of the previous subsection, this confusion matrix corresponds to approximately the same accuracy (99.8 percent), an improved recall (70.5 to 78.6 percent), a worsened precision (72.2 to 65.7 percent), and approximately the same F1 score (71.3 to 71.6 percent).

The following chapter offers a discussion on the algorithms' performance and their application to PoL anomaly detection.

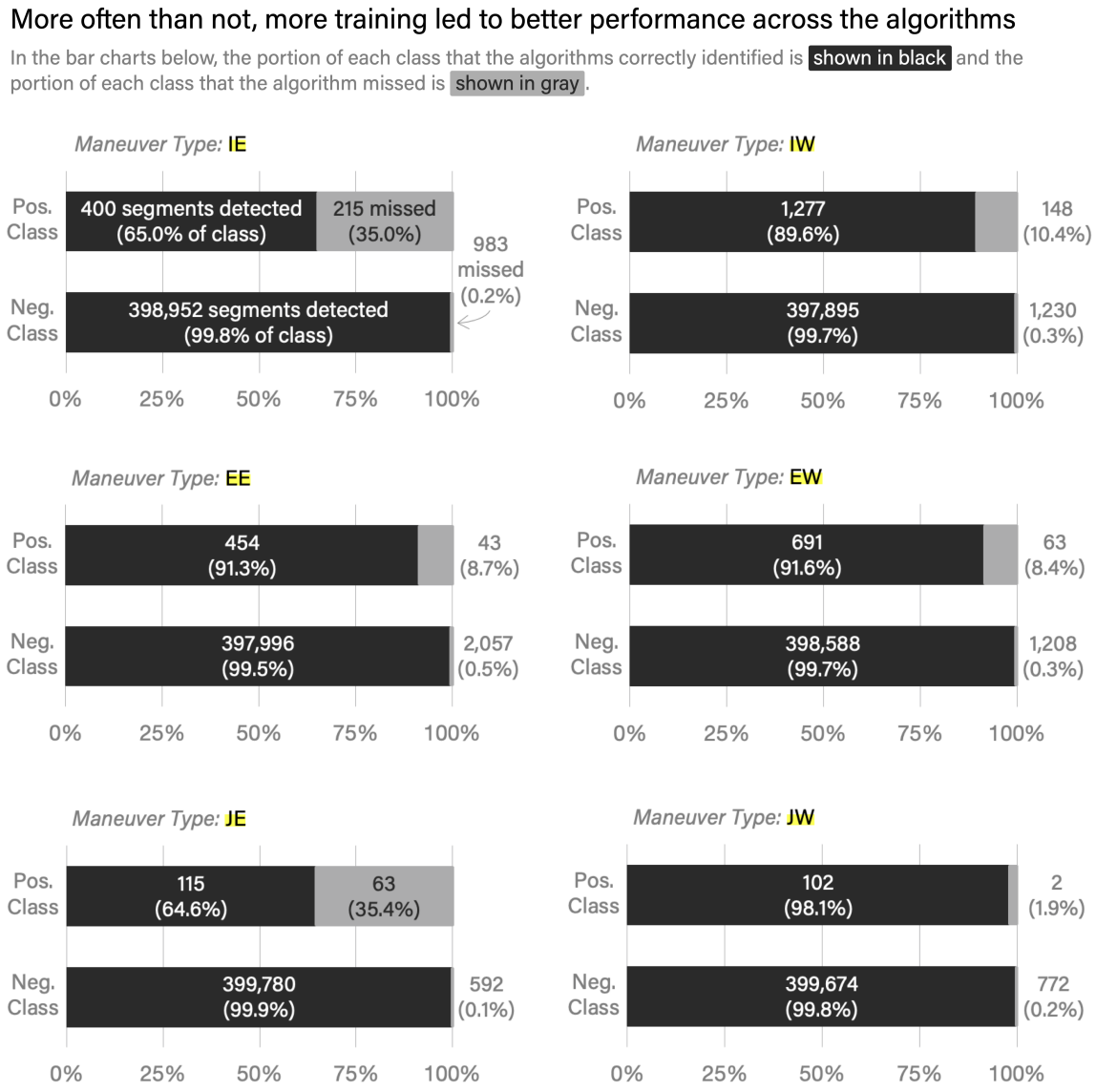

Figure 4-4: Performance metrics for the suite of satellite maneuver detection algorithms on a segment-by-segment basis after training on ten years' worth of GEO satellite data. The true positive and false negative portions of the confusion matrices are shown in the positive class of each bar chart in black and gray, respectively. The true negative and false positive portions of the confusion matrices are shown in the negative class of each bar chart in black and gray, respectively.

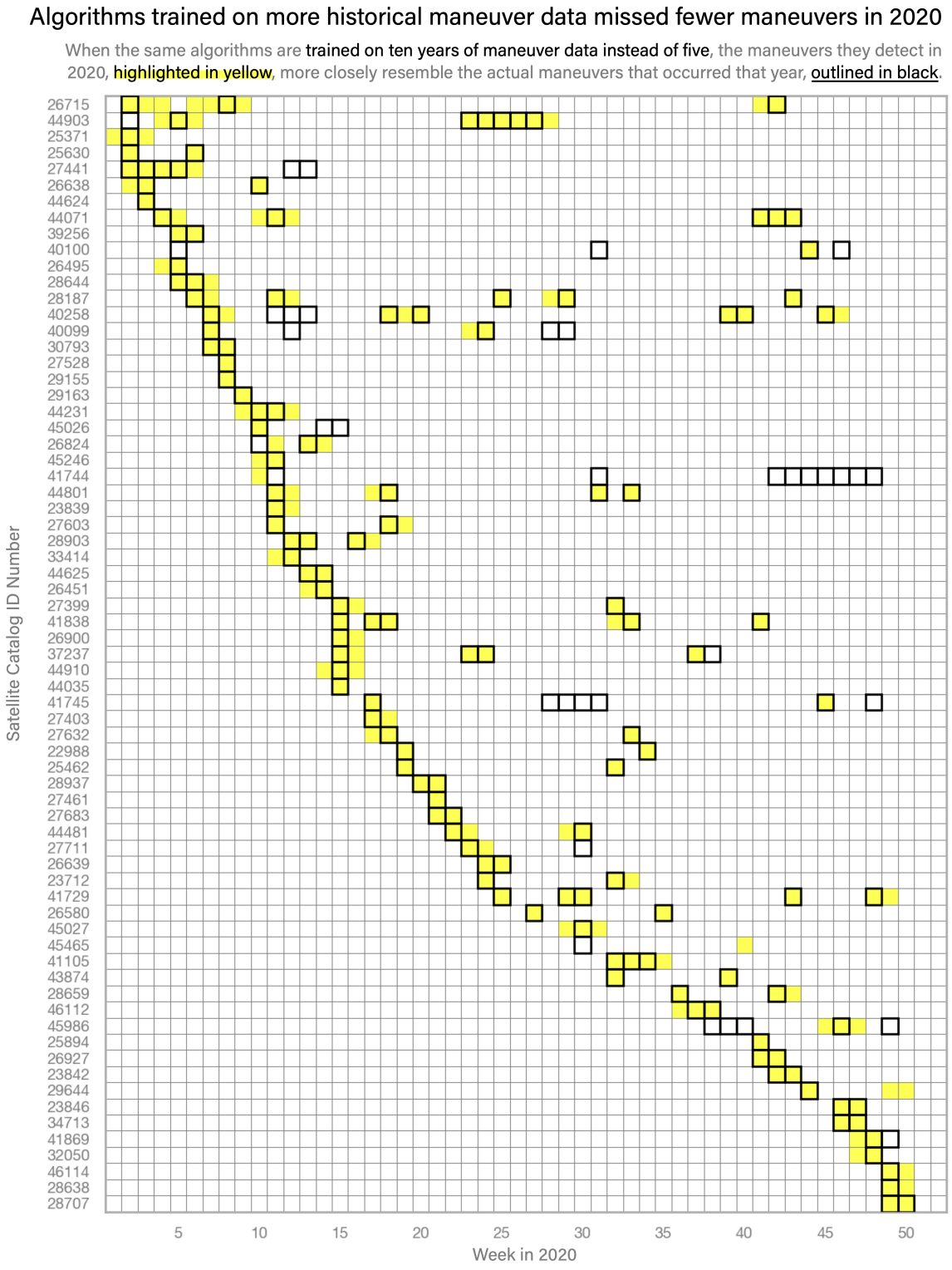

Figure 4-5: Detection results for the suite of satellite maneuver detection algorithms on a maneuver-by-maneuver basis after training on ten years' worth of GEO satellite data. The rows of the figure correspond to the 71 GEO satellites that performed a longitudinal shift maneuver of any kind in 2020 ordered by the week of their first maneuver.

Chapter 5

Discussion

The performance metrics for the two suites of algorithms described in the previous chapter—accuracy, recall, precision, and the F_1 score—demonstrate the algorithms' promise for anomaly detection in GEO. The following sections describe various examples of both nominal and anomalous satellite behavior from the 2020 test dataset and whether or not they can be identified using the results presented in the previous chapter.

5.1 Identifying Nominal and Anomalous Satellite Retirement

When satellites reach the end of their operational lifetime, they are often removed from GEO and placed in GYO, as described in Section 1.2 and shown in Figure 2-1. Thus, the act of retiring a satellite may be considered nominal behavior for relatively old satellites, but anomalous behavior for younger ones.

Figure 5-1 shows a portion of a satellite's longitudinal position history that includes a retirement maneuver. The satellite, *Thaicom 5* (Satellite ID: 29163), was launched in May 2006 and performed no longitudinal shift maneuvers until its retirement in late February 2020. With almost fourteen years of station-keeping in GEO, *Thaicom 5*'s detected retirement could be considered nominal behavior. Both suites of algorithms described in the previous chapter—the one trained on 5 years' worth of GEO satellite maneuver data and the one trained on 10—were successful in detecting the IW maneuver associated with the retirement of *Thaicom 5*.

The pair of algorithm suites did not perform equally well, however, in identifying the anomalous retirement of DirecTV's *Spaceway 1* (Satellite ID: 28644). Only the suite of algorithms trained on 10 years' worth of GEO satellite maneuver data successfully detected

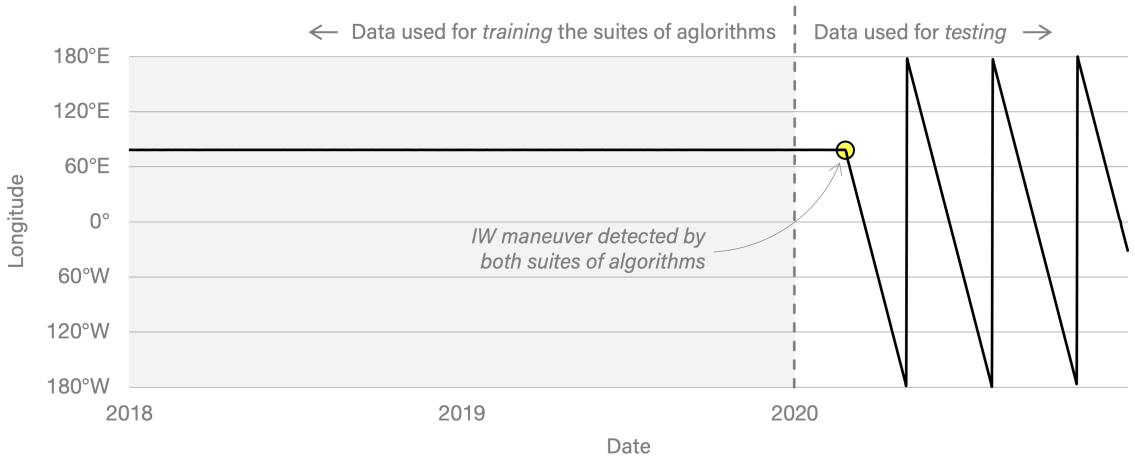

Figure 5-1: Maneuver detection results for Thaicom's *Thaicom 5*. This figure shows daily longitudinal positions for Thaicom's *Thaicom 5* (Satellite ID: 29163) from January 1, 2018, to December 31, 2020. The satellite was launched on May 27, 2006, and occupied approximately the same longitudinal position, 78.4°E, from July 2006 until its retirement in February 2020. Both suites of satellite manuever detection algorithms—the one trained on 5 years' worth of GEO satellite maneuver data and the one trained on 10—correctly detected the IW maneuver.

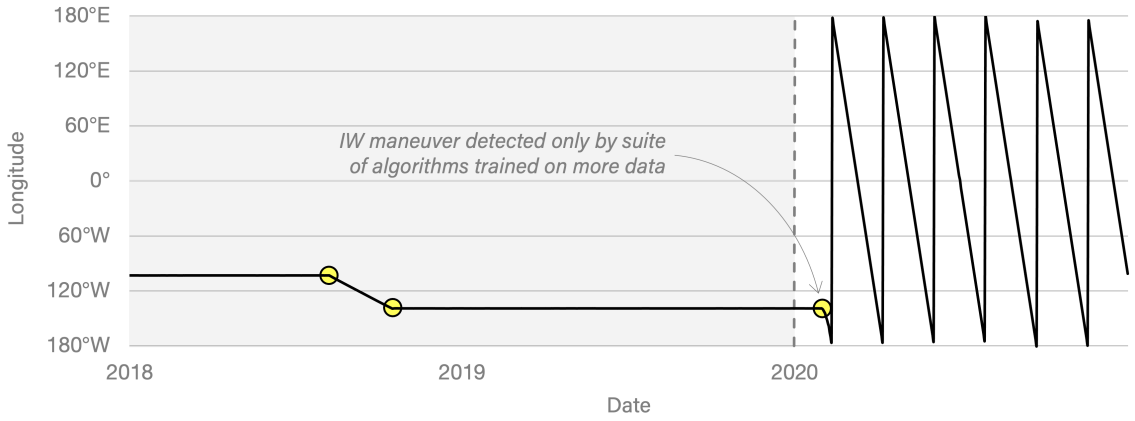

Figure 5-2: Maneuver detection results for DirecTV's *Spaceway 1*. This figure shows daily longitudinal positions for DirecTV's *Spaceway 1* (Satellite ID: 28644) from January 1, 2018, to December 31, 2020. The satellite was launched on April 26, 2005, and occupied one longitudinal position, 102.8°W, from August 2005 to August 2018, and a second position, 138.9°W, from October 2018 until its retirement in late January and early February 2020.

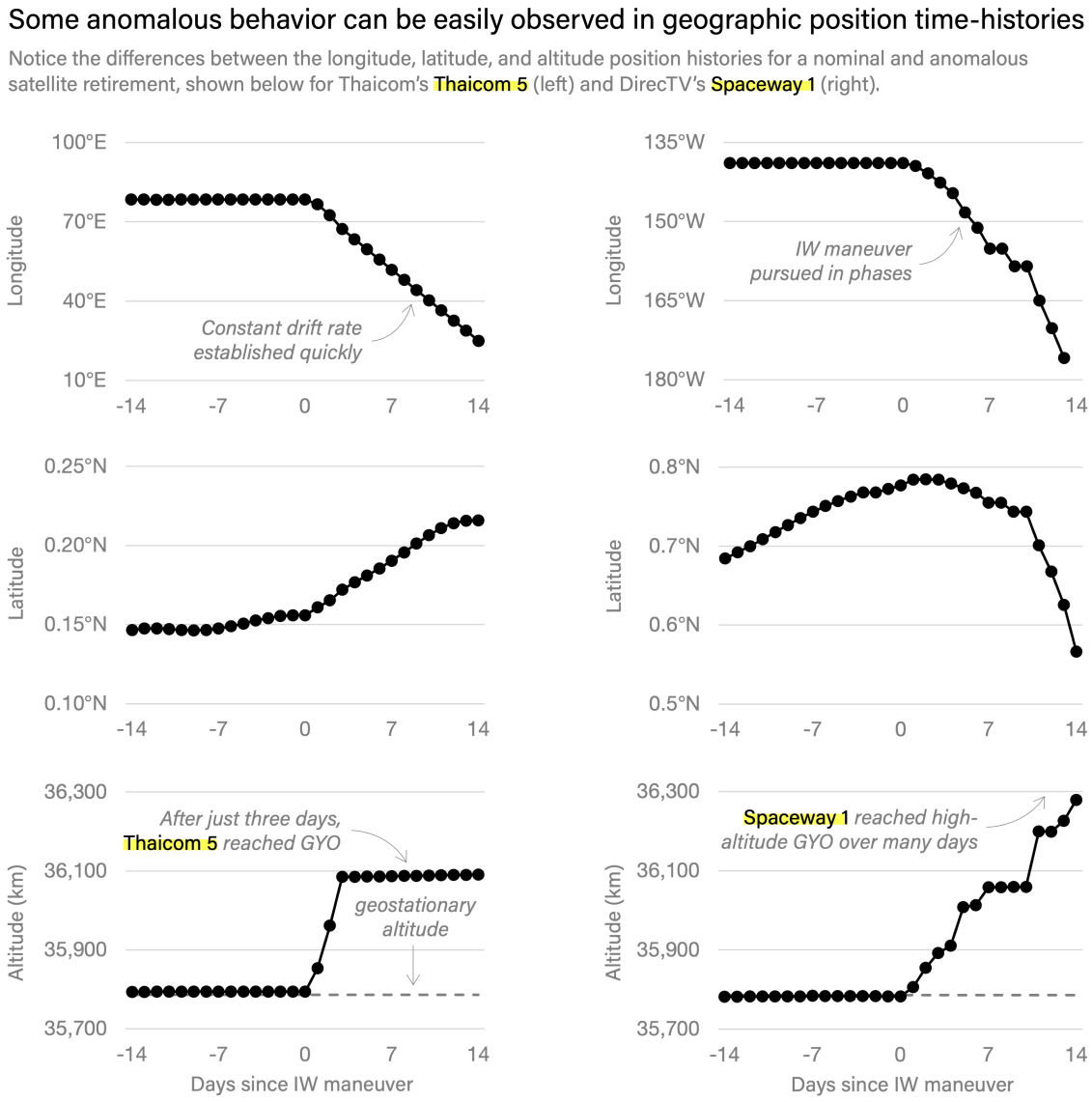

Figure 5-3: Comparing *Thaicom 5*'s and *Spaceway 1*'s geographic position histories. *Thaicom 5*'s nominal retirement is shown in the left three subplots and *Spaceway 1*'s anomalous retirement is shown in the right three subplots. Although there are noticeable differences between the two satellites in each of the three geographic coordinate time-histories, the most obvious ones perhaps come from a comparison of the two satellites' altitudes before and after the beginning of their retirement maneuvers, shown in the bottom-left and bottom-right subplots. While *Thaicom 5*'s retirement maneuver to the graveyard orbit took just three days, *Spaceway 1*'s maneuver took longer and resulted in an altitude approximately 500 km above geostationary altitude, much higher than a standard graveyard orbit, like *Thaicom 5*'s.

the IW maneuver associated with the satellite's retirement, shown in Figure 5-2.

Although *Spaceway 1* retired nearly 15 years after its launch in April 2005—meaning it had a longer operational lifetime than other GEO satellites, including *Thaicom* 5—it did so in response to an on-orbit malfunction, not simply because it reached the end of its operational lifetime [20]. According to the operator, the satellite's onboard batteries suffered "significant and irreversible thermal damage" as part of an anomaly detected in December 2019 that led to "a significant risk that [the] battery cells could burst" [46]. After receiving permission from the U.S. Federal Communications Commission to skip the standard guidelines surrounding expending all remaining fuel at the end of a satellite's operational lifetime, DirecTV rapidly decommissioned the satellite on short notice [37]. The IW maneuver associated with *Spaceway 1*'s non-standard retirement was only detected by the suite of algorithms trained on 10 years' worth of historical GEO maneuver data. The suite trained on only 5 years of data did not detect it. Figure 5-3 offers a more detailed view of the two satellites' geographic positions for several days before and after each of their retirement maneuvers.

The subplots in Figure 5-3 show the differences between *Thaicom 5*'s nominal retirement and *Spaceway 1*'s anomalous one. *Thaicom 5*'s IW maneuver was brief; it took only three days to move from geostationary altitude (shown in the left hand side of the bottom-left subplot) to the graveyard orbit. *Spaceway 1*'s retirement, on the other hand, occurred over several days; eventually the satellite was placed in a graveyard orbit more than 500 km above geostationary altitude, a higher-than-average orbit for a retired satellite. Since there are fewer historical examples of satellite retirements like *Spaceway 1*, training on more historical data helped the suite of maneuver detection algorithms detect the IW maneuver associated with its retirement.

5.2 Identifying Nominal and Anomalous Longitudinal Shifts

The suite of maneuver detection algorithm designed in Section 3.3 and evaluated in Section 4.1 was principally designed to detect longitudinal shift maneuvers. This subsection describes several examples of longitudinal shift maneuvers that occurred in the 2020 test dataset, how they could be considered nominal or anomalous, and whether or not the two suites of algorithms detected them.

When satellites perform a longitudinal shift maneuver, their previous PoL—the description of their behavior prior to the maneuver taking place—can help determine the nominal or anomalous nature of the maneuver. Figures 5-4, 5-5, and 5-6 show the longitudinal

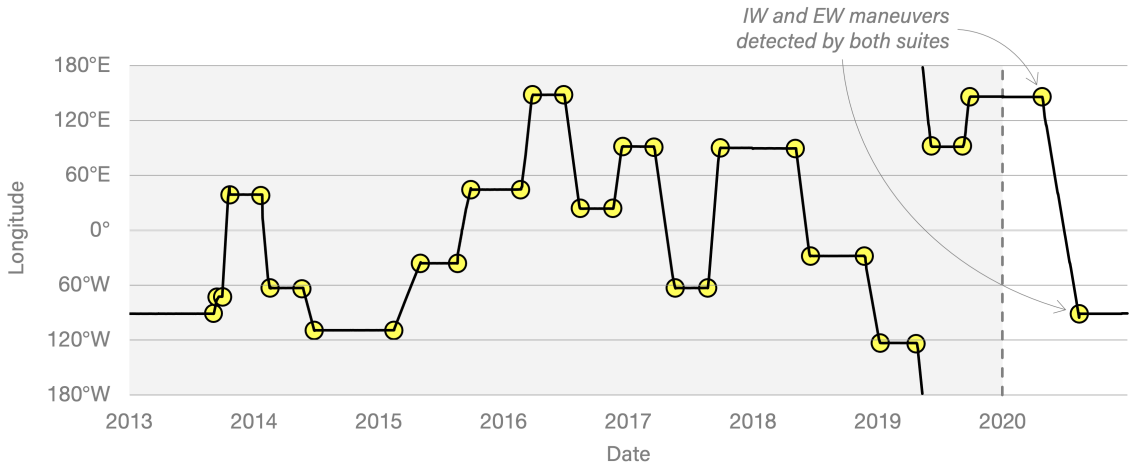

Figure 5-4: Maneuver detection results for Telesat's *Nimiq 2*. This figure shows daily longitudinal positions for Telesat's *Nimiq 2* from January 1, 2013, to December 31, 2020. The satellite was launched on December 29, 2002, and has occupied at least 16 longitudinal positions in GEO since then, making it one of the most maneuvered satellites in the SPACECOM space object catalog. In 2020, the satellite performed a longitudinal maneuver with a longer drift period than ever before, but a familiar drift rate.

position histories for Telesat's *Nimiq 2*, DirecTV's *Spaceway 2* (Satellite ID: 28903), and the U.S. Air Force's *Wideband Global Satcom 2* (Satellite ID: 34713), respectively.

Telesat's *Nimiq 2* satellite has performed more longitudinal shift maneuvers than almost any other GEO satellite in the SPACECOM space object catalog. In 2020, it performed a westward shift maneuver. Although the maneuver featured a longer drift period than that of any previous longitudinal shift maneuver, the satellite's drift rate was approximately equal to those previous. Since the satellite's 2020 behavior largely adheres to its previous PoL, the newest maneuver can be considered nominal. Both the 5-year and 10-year satellite maneuver detection algorithm suites detected the IW and EW maneuvers that *Nimiq 2* performed in 2020.

DirecTV's *Spaceway 2*, on the other hand, performed no longitudinal shift maneuvers of any kind after it launched in November 2005 until March 2020, when it shifted westward by almost 40 degrees longitude. Although the drift rate associated with this maneuver is similar to many other satellites' drift rates, the fact that it maneuvered at all was at odds with the satellites' previous PoL. Because of this difference, the maneuver could be considered anomalous. Both suites of maneuver detection algorithms successfully detected the IW and EW maneuvers from 2020.

Just like *Spaceway 2*, the U.S. Air Force's *Wideband Global Satcom 2 (WGS F2)* performed no longitudinal shift maneuvers after its launch in April 2009 until November 2020.

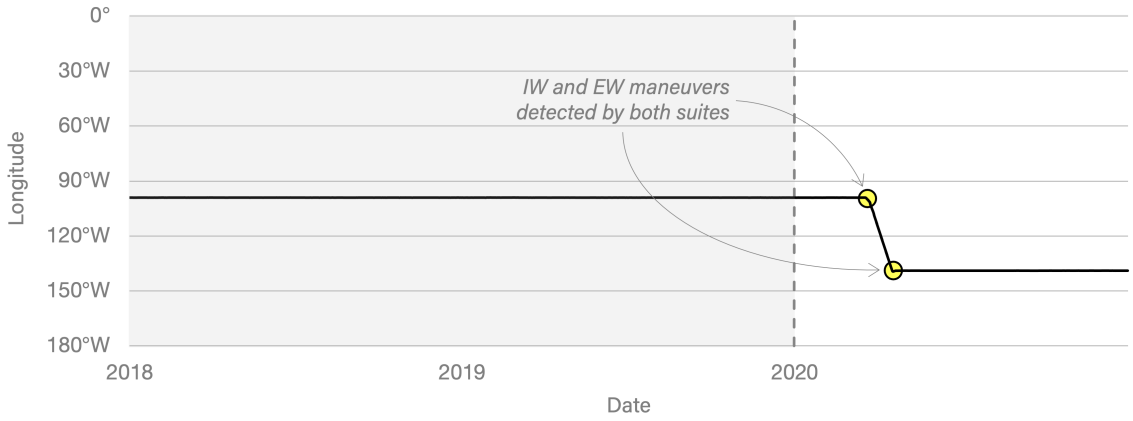

Figure 5-5: Maneuver detection results for DirecTV's *Spaceway 2*. This figure shows daily longitudinal positions for DirecTV's *Spaceway 2* (Satellite ID: 28903) from January 1, 2018, to December 31, 2020. The satellite was launched on November 16, 2005, and occupied approximately the same longitudinal position, 99.2°W, from February 2006 until it performed a westward longitudinal shift maneuver in March and April 2020.

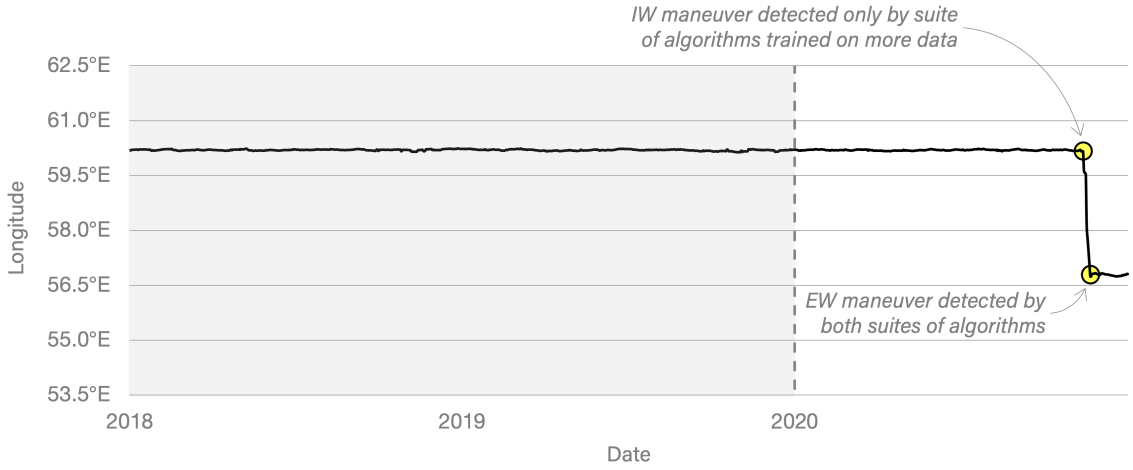

Figure 5-6: Maneuver detection results for the U.S. Air Force's *WGS F2*. This figure shows daily longitudinal positions for the U.S. Air Force's *WGS F2* (Satellite ID: 34713) from January 1, 2018, to December 31, 2020. The satellite was launched on April 4, 2009, and occupied approximately the same longitudinal position, 60.2°E, from the beginning of its geographic position time-history until it performed a westward longitudinal shift maneuver in November 2020.

Similarly, because the satellite's 2020 behavior differs from its previous PoL, its westward longitudinal shift maneuver could be considered anomalous. Unlike *Spaceway 2*, however, the maneuver was difficult to detect by the suites of machine learning algorithms, possibly due to its relatively small longitudinal displacement: less than 4 degrees over the course of nine days. Although both the suite of algorithms trained on 5 years of historical data and 10 years detected the EW maneuver associated with the end of *WGS F2*'s 2020 westward shift maneuver, only the suite trained on more data caught the IW maneuver.

5.3 Well-known Cases of Anomalous Behavior in GEO

Some satellites in GEO have unique missions that lead to PoLs unlike any others. This subsection describes three examples of satellites that are well known for their anomalous behavior in GEO and whether or not the two suites of algorithms detected their maneuvers in 2020.

Figures 5-7, 5-8, and 5-9 show the longitudinal position histories for Russia's *Luch (Olymp)* (Satellite ID: 40258), China's *SJ-17* (Satellite ID: 41838), and Space Logistics' *MEV-1* (Satellite ID: 44625), respectively.

Luch (Olymp) is a Russian GEO satellite that was launched in September 2014. Since then, it has occupied over 20 longitudinal positions in the geostationary belt—more than any other GEO satellite in the SPACECOM space object catalog—and approached several uncooperative satellites in the process, attracting attention from the international space community [42]. Unlike other satellites that perform many maneuvers, most of *Luch*'s longitudinal shift maneuvers were small, as shown in the top subplot of Figure 5-7. For the majority of *Luch*'s on-orbit lifetime, the satellite has shifted eastward in the geostationary belt, forming a stair-step pattern in its longitudinal position history from the beginning of 2016 to the end of 2019. In 2020, however, *Luch* abandoned this unique PoL and performed two westward longitudinal shifts with relatively long drift periods, among others. The bottom subplot of Figure 5-7 describes *Luch*'s behavior during the year 2020. As the figure shows, the two suites of maneuver detection algorithms both detected a majority of the maneuvers performed by *Luch* in 2020, including the initial IW maneuver that indicated that the satellite was deviating from its previous PoL, but failed to correctly identify a cluster of maneuvers (EW, IE, and EE) that were labeled consecutively. Since this cluster of maneuvers is exceedingly rare—it never appeared in the 5- or 10-year training dataset under the labeling strategy described in Subsection 3.3.1—the algorithms were not trained well enough to detect it.

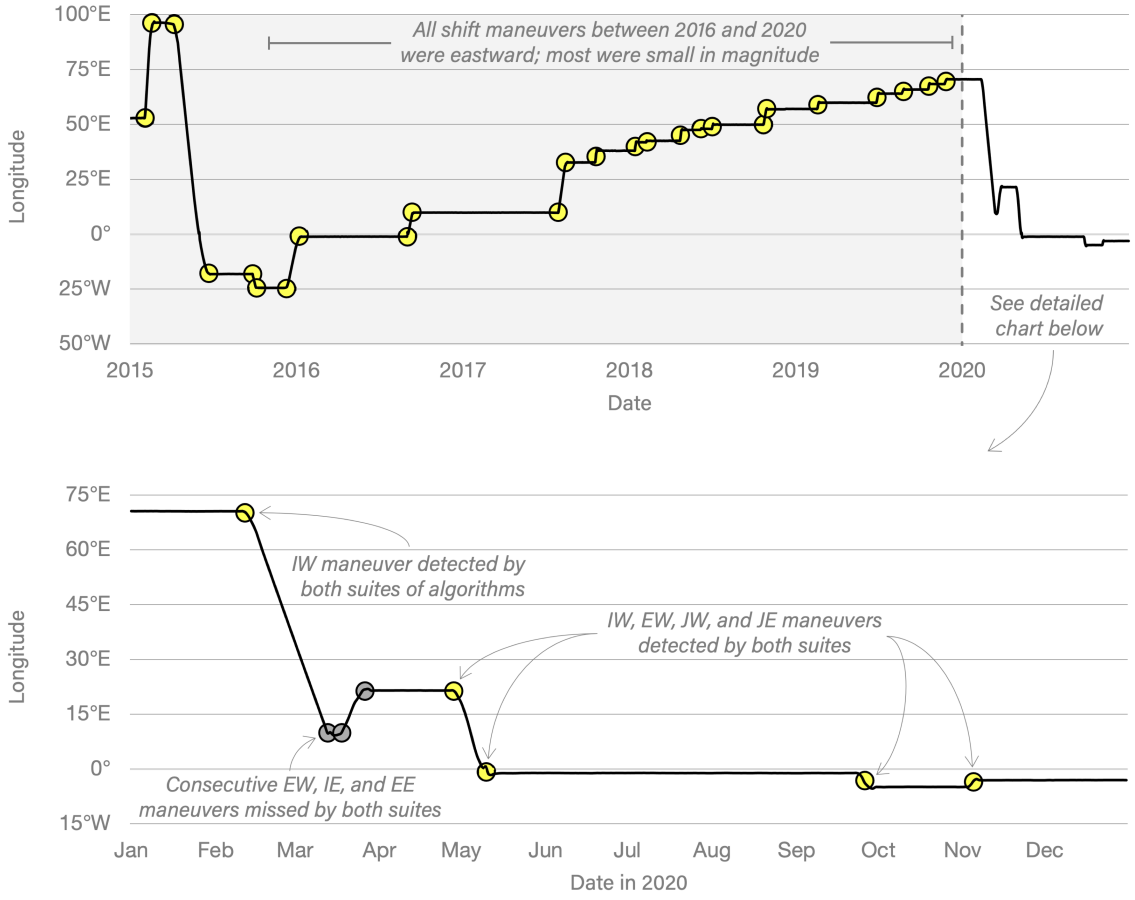

Figure 5-7: Maneuver detection results for Russia's *Luch (Olymp)*. The top subplot of this figure shows daily longitudinal positions for Russia's *Luch (Olymp)* (Satellite ID: 40258) from January 1, 2015, to December 31, 2020. The satellite was launched on September 27, 2014, and has occupied more than 20 longitudinal positions in GEO since then, making it one of the most maneuvered satellites in the SPACECOM space object catalog. In 2020, the satellite performed a variety of longitudinal shift maneuvers, which can be seen in greater detail in the bottom subplot.

SJ-17 is a Chinese GEO satellite that was launched in November 2016. Like *Luch*, *SJ-17* has performed several close approaches during its time in orbit [43]. Unlike *Luch*, many of the satellites approached by *SJ-17* have been Chinese, and likely cooperative partners in various rendezvous and proximity operations [16]. In addition to its pattern of regular close approaches, *SJ-17*'s behavior is also unique in the way it performs its longitudinal shift maneuvers. The satellite has a pattern of adjusting its drift rate during drift periods, creating additional discontinuities in its longitudinal history plot. Despite this pattern continuing into 2020, both suites of maneuver detection algorithms successfully detected all four of the maneuvers labeled in the 2020 test dataset and did not label the discontinuity in the August 2020 westward drift as a maneuver.

MEV-1 is a U.S. GEO satellite built by Northrop Grumman and operated by Space Logistics, LLC, that launched in October 2019. Also known as *Mission Extension Vehicle-1*, *MEV-1* became the first satellite to offer mission extension services to another satellite in GEO in February 2020 when it docked with Intelsat's *Intelsat 901* (Satellite ID: 26824), a retired satellite in a graveyard orbit, and later returned it to the geostationary belt [35]. Because of this mission, *MEV-1*'s PoL is perfectly backwards when compared to the vast majority of other GEO satellites: its geographic position history shows the satellite starting in a high-altitude graveyard orbit and ending in the geostationary belt. Although this type of behavior is highly unusual, both suites of maneuver detection algorithms detected the corresponding EE maneuver in 2020, as it resembles many other maneuvers when observed in the context of a short geographic time-history segment.

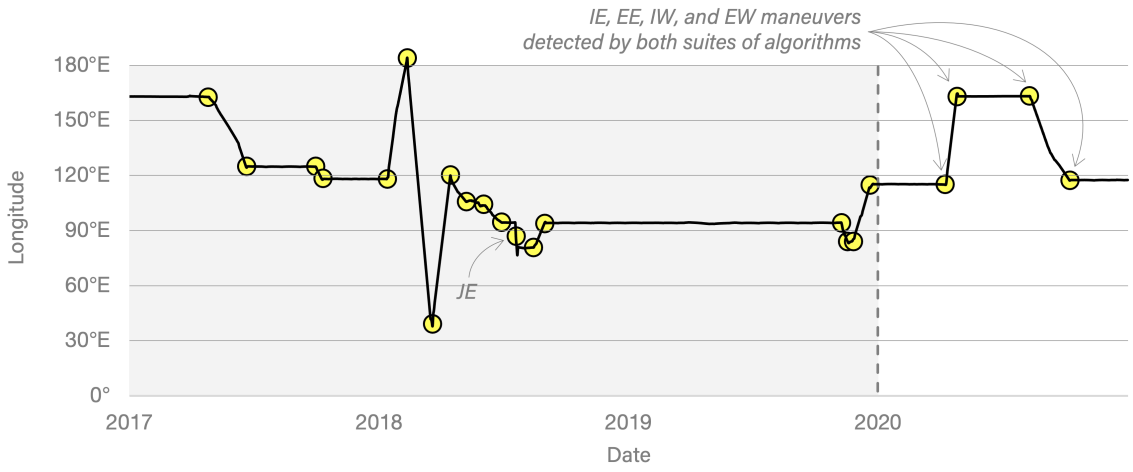

Figure 5-8: Maneuver detection results for China's *SJ-17*. This figure shows daily longitudinal positions for China's *SJ-17* (Satellite ID: 41838) from January 1, 2017, to December 31, 2020. The satellite was launched on November 3, 2016, and has pursued a variety of longitudinal shift maneuvers since then, including several with unusual drift patterns in which the satellite adjusted its drift rate during drift periods. In 2020, the satellite performed a variety of longitudinal shift maneuvers, including one westward longitudinal shift in which the drift rate was adjusted before the maneuver was completed.

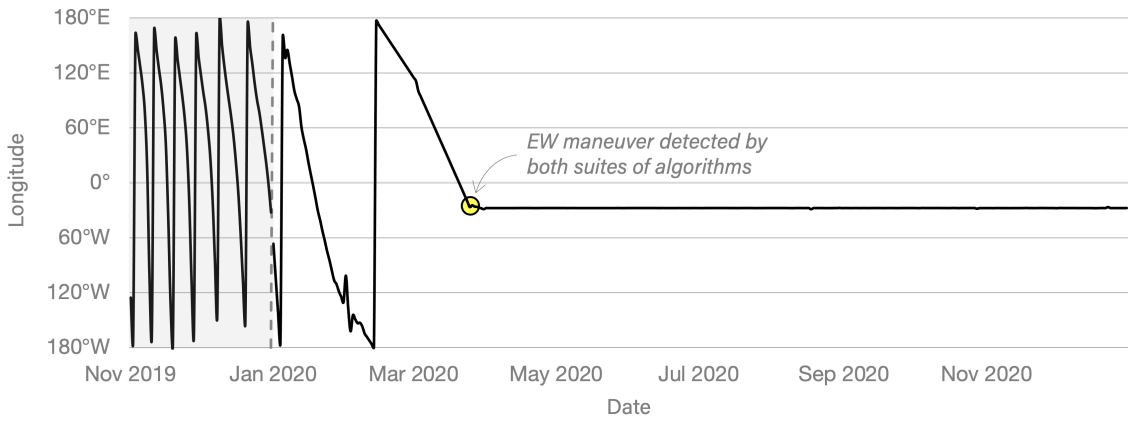

Figure 5-9: Maneuver detection results for Space Logistics' *MEV-1*. This figure shows daily longitudinal positions for Space Logistics' *MEV-1* (Satellite ID: 44625) from November 1, 2019, to December 31, 2020. Although the satellite was launched on October 9, 2019, it did not enter the geostationary belt until several months later in March 2020. *MEV-1* spent the first few months of its operational lifetime in the graveyard orbit, where it docked with Intelsat's *Intelsat 901* (Satellite ID: 26824) and later maneuvered to the geostationary belt.

Chapter 6

Policy Applications

Because of its performance and replicability, the method described in this work as well as a number of its data byproducts—such as the longitudinal shift maneuver database used for algorithm training and the geographic position histories created for all satellites in GEO—have the potential to contribute to several interesting efforts in international relations in space. This chapter offers several such examples, including the allocation of space domain resources and developing norms of behavior for on-orbit satellite operations.

6.1 Studying Compliance with Guidelines and Agreements

In November 2019, the U.S. Government updated its orbital debris mitigation guidelines, which included revised standard practices for post-mission behavior for GEO satellites [1]. According to the new guidelines, GEO satellites should be removed from the geostationary belt at the end of their operational lifetime such that their perigee remains more than 200 km above geostationary altitude for at least 100 years.[1] Additionally, in an effort to minimize "the risk to other space systems from accidental explosions and associated orbital debris after completion of mission operations," all GEO satellites should deplete their onboard propellant and compressed gases once they reach their disposal orbit, according to the guidelines.

The method for detecting satellite maneuvers in GEO described in the previous chapters could contribute to compliance verification for both post-mission disposal of GEO satellites and onboard propellant depletion. Post-mission disposal can easily be detected by this

[1]Note that this implicit definition of GYO differs from the one used in Chapters 2 and 3, which was 300 km above geostationary altitude.

method, as discussed in Chapter 5. The detection of satellite maneuvers of any kind after a satellite reaches its post-mission disposal orbit could suggest the violation of the standard practice of onboard propellant depletion, since some propellant must be expended in order to perform a maneuver.

Unlike operators in other orbital regimes, satellite operators in GEO must acquire a license to operate in the domain from the International Telecommunications Union (ITU), a specialized agency of the United Nations [44]. Licenses from the ITU—which describe a portion of the geostationary belt, known as an *orbital slot*, and a portion of the radio-frequency spectrum, known as a *frequency band*, in which satellites can operate—ensure satellites in GEO have both the physical and spectral space they need to function without harmful radio-frequency interference from neighboring space systems [39]. When satellites perform longitudinal shift maneuvers with a significant longitudinal displacement, they are almost certainly switching orbital slots in the process, which presents challenges when it comes to adhering to ITU license agreements. Detecting such maneuvers is of critical importance to regulators tasked with studying compliance to the ITU's guidelines and evaluating future license applications from operators with previous violations.

The history of compliance with both the United States' and ITU's guidelines, which can be studied using the geographic position time-histories created for GEO satellites as part of this study, can help inform the development of future space sustainability practices and orbital allocation processes both in GEO and other orbital regimes.

6.1.1 Verifying Claims of Unusual Behavior

This work can also contribute to the verification of public claims of particularly nefarious satellite behavior, even when it is denied by perpetrators.

In September 2018, the French defense minister claimed that a Russian satellite, *Luch (Olymp)*, performed an uncoordinated close approach with a French-Italian military satellite, *Athena-Fidus* (Satellite ID: 39509) [28]. Such an action would likely constitute both a violation of ITU license agreements [32] and represent unfavorable behavior within the international space community or an "act of espionage" according to the defense minister. Detecting longitudinal shift maneuvers, as demonstrated for this particular Russian satellite in Figure 5-7, could help verify France's claim and form the basis of new norms that would prevent future uncoordinated close approaches.

6.2 Developing Future Norms of Behavior

Perhaps the most important contribution of this work to the international space policy community is its potential to form a quantitative basis for the development of future norms of behavior in GEO, including guidance on best practices for longitudinal shift maneuvers and a minimum separation distance between noncooperative satellites [44].

The products of this work—an algorithmic method for detecting longitudinal shift maneuvers and a record of previous maneuvers in an easily interpretable coordinate system—could help form the basis of guidelines surrounding how to perform longitudinal shift maneuvers without interfering with neighboring satellites' activities. The history of GEO satellite operations described in each satellite's geographic position history provides hundreds of examples of how operators choose to pursue maneuvers in the absence of agreed-upon rules and guidelines, which could inform the design of new ones. Additionally, detecting longitudinal shift maneuvers could trigger the investigation of potentially uncoordinated close approaches, which threaten satellites with on-orbit collision and other, non-kinetic types of attacks. A future norm to prevent close approaches, such as setting a minimum separation distance for noncooperative satellites, could be both informed and verified via satellite maneuver detection.

THIS PAGE INTENTIONALLY LEFT BLANK

Chapter 7

Conclusion

The results presented in Chapter 4 and discussed in Chapter 5 demonstrate the promise of using supervised machine learning techniques to detect longitudinal shift maneuvers in GEO. Since TLE data is a publicly available resource, this work can be replicated regardless of a researcher's access to other, likely more proprietary space object orbital data, which can make it more easily applicable to policy debates, like those discussed in Chapter 6.

Because this method depends on manually labeling satellite behavior based on geographic position time-histories, it is more limited than some of the other methods cited in Section 2.2. Although satellite behavior can easily be discerned by inspecting historical geographic coordinates for objects in GEO, as shown in Figure 1-2, discerning behavior in other orbital regimes in this way is more challenging. In LEO and MEO, for example, satellite positions in latitude and longitude space is rapidly changing over time; inspecting the time-histories of other orbital parameters will likely yield more accurate results. That being said, the dependence on geographic coordinates could continue to be a strength for detecting other interesting behavior in GEO besides longitudinal shift maneuvers, such as identifying and predicting station-keeping maneuvers or classifying satellites' PoLs.

Regardless of the types of behavior being detected with this methodology, the algorithm designed in Section 3.3 would likely benefit from hyperparameter tuning, which may lead to more favorable performance metrics than those presented in Chapter 4.

This work both develops and demonstrates a novel method for detecting satellite behavior in GEO, with great potential for other applications, both in on-orbit satellite behavior analysis and developments in international space policy.

THIS PAGE INTENTIONALLY LEFT BLANK

Appendix A

Acronyms and Abbreviations

Abbreviation	Full Name or Definition
18 SPCS	18th Space Control Squadron
ADASYN	Adaptive Synthetic Sampling Approach for Imbalanced Learning
CNN	Convolutional Neural Network
EE	End Eastward Drift; a component of a longitudinal shift maneuver
ESA	European Space Agency
EUMETSAT	European Organization for the Exploitation of Meteorological Satellites
EW	End Westward Drift; a component of a longitudinal shift maneuver
FN	False Negative; an element of the binary confusion matrix
FP	False Positive; an element of the binary confusion matrix
GEO	Geosynchronous orbital regime
GOES	Geostationary Operational Environmental Satellite
IADC	Inter-Agency Space Debris Coordination Committee
IE	Initiate Eastward Drift; a component of a longitudinal shift maneuver
IW	Initiate Westward Drift; a component of a longitudinal shift maneuver

Continued on next page

Table A.1: Acronyms and abbreviations. This table offers the full name or definition for the acronyms and abbreviations referenced in this work.

Continued from previous page

Abbreviation	Full Name or Definition
ITU	International Telecommunications Union
JE	Jump Eastward; a type of longitudinal shift maneuver
JW	Jump Westward; a type of longitudinal shift maneuver
LEO	Low Earth Orbit
MEO	Medium Earth Orbit
NASA	National Aeronautics and Space Administration
NOAA	U.S. National Oceanic and Atmospheric Association
PoL	Pattern of Life
ReLU	Rectified Linear Unit; an activation function
SMOTE	Synthetic Minority Oversampling Technique
SPACECOM	U.S. Space Command
SSA	Space Situational Awareness
TLE	Two-line Element
TN	True Negative; an element of the binary confusion matrix
TP	True Positive; an element of the binary confusion matrix
USSF	United States Space Force

Appendix B

Referenced GEO Satellites

ID	Name	Launch Date	Operator
858	*Syncom 3*	Aug. 19, 1964	NASA (United States)
10000	*OPS 9437*	May. 12, 1977	U.S. Air Force (United States) [13]
11648	*Gorizont 3*	Dec. 28, 1979	Russian Satellite Communications Company (Russia) [14]
11964	*GOES-4*	Sep. 9, 1980	NOAA (United States)
24932	*Meteosat 7*	Sep. 2, 1997	EUMETSAT (ESA)
26824	*Intelsat 901*	Jun. 9, 2001	Intelsat (United States)
27509	*Meteosat 8*	Aug. 28, 2002	EUMETSAT (ESA)
27632	*Nimiq 2*	Dec. 29, 2002	Telesat Canada Ltd. (Canada)
28644	*Spaceway 1*	Apr. 26, 2005	DirecTV, Inc. (United States)
28903	*Spaceway 2*	Nov. 16, 2005	DirecTV, Inc. (United States)
29163	*Thaicom 5*	May. 27, 2006	Thaicom (Thailand)
33414	*VeneSat-1*	Oct. 29, 2008	Ministry of Science and Technology (Venezuela) [15]

Continued on next page

Table B.1: Referenced GEO satellites. This table features the name, SPACECOM catalog ID number, launch date, and operator for each GEO satellite referenced in this work using data retrieved from SatelliteDashboard.org [47] unless otherwise noted.

Continued from previous page

ID	Name	Launch Date	Operator
34713	*WGS F2*	Apr. 4, 2009	U.S. Air Force (United States)
39509	*Athena-Fidus*	Feb. 6, 2014	Centre National d'Etudes Spatiales (France) / Agenzia Spaziale Italiana (Italy)
40258	*Luch*	Sep. 27, 2014	Ministry of Defense (Russia)
41308	*Intelsat 29e*	Jan. 27, 2016	Intelsat (United States)
41838	*SJ-17*	Nov. 3, 2016	China Satellite Communication Corportation (China)
44625	*MEV-1*	Oct. 9, 2019	Space Logistics, LLC (United States)

Appendix C

Notes on Data Cleaning

This appendix describes the data cleaning efforts associated with this work, including the steps taken in response to encoding errors identified in TLE data from the SPACECOM space object catalog [53] and processing errors from commands associated with the PyEphem Python library [40].

C.1 TLE Encoding Errors

Because TLEs encode orbital parameters and other space object information within two relatively long strings of characters, as opposed to using delimited lists, they are prone to human errors during transcription. In some cases, such as an obviously misplaced space character, the error can be identified and corrected. In other cases, when the error can not be identified, the erroneous TLE can simply be removed from a satellite's TLE time-history.

One common TLE error is an *extra* space character before the "epoch" field and a *missing* space character before the "element set number" field. Although a TLE with this error is unreadable by the PyEphem Python library, it can be easily fixed by moving the space character to its correct position. This particular solution was used for 553 TLEs describing the behavior of 21 GEO satellites in this study.

For one TLE, the "revolution number at epoch" field was described using too many characters. Since the solution to this error could not be identified with certainty, the TLE was removed from its satellite's TLE time-history.

C.2 Insufficient or Implausible Orbital Data

After completing the process of identifying GEO satellites described in Section 3.1, it may become clear that not all space objects identified using this method should be considered GEO satellites. Although there were 1,128 objects in the SPACECOM catalog at the time it was accessed for this work with at least one TLE corresponding to an orbit within the geosynchronous region as defined by the IADC, 19 were removed due to insufficient or implausible orbital data. In a few cases, satellites have only a handful of TLEs in their TLE time-history. In others, the vast majority of a satellite's TLE time-history places it in another orbital regime entirely, with the exception of one or two GEO TLEs. These cases are likely due to a concept known as *cross-tagging*, where passively observed objects are mislabeled after one passes behind another in a space surveillance sensor's reference frame [33, 68]. These satellites were removed from this study, meaning their longitudinal shift maneuver history was not labeled, nor used for training the satellite maneuver detection algorithms.

C.3 PyEphem RunTime Errors

The PyEphem Python library is used to calculate GEO satellites' positions in geographic coordinates more than 8,000,000 times for this work. Occasionally, the library exhibits a RunTime error when it loads a TLE and attempts to calculate its geographic position at a given time. This error was produced 120 times across 79 satellites in this study. Since the errors were so rare, the affected geographic position data points were simply removed, and not used as part of the training or testing data sets.

Bibliography

[1] U.S. Government Orbital Debris Mitigation Standard Practices, November 2019 Update. Technical report, 2019. URL: https://orbitaldebris.jsc.nasa.gov/library/usg_orbital_debris_mitigation_standard_practices_november_2019.pdf.

[2] X. Bai, C. Liao, X. Pan, and M. Xu. Mining Two-Line Element Data to Detect Orbital Maneuver for Satellite. *IEEE Access*, pages 129537–129550, 2019. doi:10.1109/ACCESS.2019.2940248.

[3] N. Brady. The geostationary orbit and satellite communications: concepts older than commonly supposed. *IEEE Transactions on Aerospace and Electronic Systems*, 38:1408–1409, 2002. doi:10.1109/TAES.2002.1145764.

[4] P. Branco, L. Torgo, and R.P. Ribeiro. A Survey of Predictive Modeling on Imbalanced Domains. *ACM Computing Surveys*, 49(31):31–50, 2016. doi:10.1145/2907070.

[5] CelesTrak. NORAD Two-Line Element Sets Historical Archive. URL: http://celestrak.com/NORAD/archives/.

[6] N.V. Chawla, K.W. Bowyer, L.O. Hall, and W.P. Kegelmeyer. SMOTE: Synthetic Minority Over-sampling Technique. *Journal of Artificial Intelligence Research*, 16:321–357, 2002.

[7] A.C. Clarke. Extra-terrestrial relays. *Wireless World*, pages 305–308, 1945.

[8] H.D. Curtis. *Orbital mechanics for engineering students*. Elsevier Aerospace Engineering Series. Elsevier Butterworth Heinemann, 2005.

[9] J. Decoto and P. Loerch. Technique for GEO RSO Station Keeping Characterization and Maneuver Detection. In *Advanced Maui Optical and Space Surveillance Technologies Conference*, 2015. URL: https://amostech.com/TechnicalPapers/2015/SSA/Decoto.pdf.

[10] P. DiBona, J. Foster, A. Falcone, and M. Czajkowski. Machine learning for RSO maneuver classification and orbital pattern prediction. *Advanced Maui Optical and Space Surveillance Technologies Conference*, 2019. URL: www.amostech.com.

[11] ESA Space Debris Office. Classification of Geosynchronous Objects. Technical Report GEN-DB-LOG-00211-OPS-GR, European Space Agency, Darmstadt, Germany, 2018.

[12] A. Gulli and S. Pal. *Deep Learning with Keras*. 2017.

[13] Gunter's Space Page. DSCS-2, 2021. URL: https://space.skyrocket.de/doc_sdat/dscs-2.htm.

[14] Gunter's Space Page. Gorizont 1 - 33 (11F662) / Tongastar 1 / Rimsat 1, 2 / PASI 1 / AsiaSat G / LMI-AP 1, 2, 2021. URL: https://space.skyrocket.de/doc_sdat/gorizont.htm.

[15] Gunter's Space Page. VENESAT 1 (Simon Bolivar 1), 2021. URL: https://space.skyrocket.de/doc_sdat/venesat-1.htm.

[16] T. Harrison, K. Johnson, T.G. Roberts, T. Way, and M. Young. Space Threat Assessment 2020. *Center for Strategic and International Studies*, 2020. URL: https://aerospace.csis.org/report-space-threat-assessment-2020/.

[17] H. He, Y. Bai, E.A. Garcia, and S. Li. ADASYN: Adaptive synthetic sampling approach for imbalanced learning. In *IEEE International Joint Conference on Neural Networks*, Hong Kong, China, 2008.

[18] H. He and Y. Ma. *Imbalanced Learning: Foundations, Algorithms, and Applications*. Wiley-IEEE Press, Piscataway, New Jersey, 1st edition, 2013.

[19] C. Henry. Intelsat-29e satellite suffers fuel leak, spotted drifting along GEO arc, 2019. URL: https://spacenews.com/intelsat-29e-satellite-suffers-fuel-leak-spotted-drifting-along-geo-arc/.

[20] C. Henry. DirecTV fears explosion risk from satellite with damaged battery, 2020. URL: https://spacenews.com/directv-fears-explosion-risk-from-satellite-with-damaged-battery/.

[21] C. Henry. Venezuela's flagship communications satellite out of service and tumbling, 2020. URL: https://spacenews.com/venezuelas-flagship-communications-satellite-out-of-service-and-tumbling/.

[22] Intelsat Corporate Communications. Intelsat Reports Intelsat 29e Satellite Failure, 2019. URL: https://www.intelsat.com/newsroom/intelsat-29e-satellite-failure/.

[23] Inter-Agency Space Debris Coordination Committee Steering Group and Working Group 4. IADC Space Debris Mitigation Guidelines. Technical report, 2007.

[24] R. Jehn, V. Agapov, and C. Hernández. The situation in the geostationary ring. *Advances in Space Research*, 35(7):18–32, 2005. doi:10.1016/j.asr.2005.03.022.

[25] A.B. Jenkin, M.E. Sorge, and J.P. McVey. National and International Disposal Requirements and Guidelines Applicable to GPS, 2015. URL: https://www.unoosa.org/pdf/icg/2015/icg10/02pf.pdf.

[26] T. Kelecy, D. Hall, K. Hamada, and D. Stocker. Satellite Maneuver Detection Using Two-line Element (TLE) Data. In *Advanced Maui Optical and Space Surveillance Technologies Conference*, Maui, Hawaii, 2007. URL: https://amostech.com/TechnicalPapers/2007/Modeling_Analysis_Simulation/Kelecy.pdf.

[27] M. Kuhn and K. Johnson. *Applied Predictive Modeling*. Springer, New York, New York, 1st edition, 2013. doi:10.1007/978-1-4614-6849-3.

[28] J. Leicester and S. Corbet. 'Espionage:' French defense head charges Russia of dangerous games in space. *DefenseNews*, 2018. URL: https://www.defensenews.com/space/2018/09/07/espionage-french-defense-head-charges-russia-of-dangerous-games-in-space/.

[29] S. Lemmens and H. Krag. Two-Line-Elements-Based Maneuver Detection Methods for Satellites in Low Earth Orbit. *Journal of Guidance, Control, and Dynamics*, 37:860–868, 2014.

[30] S. Lewin. Old Weather Satellite Headed to 'Graveyard Orbit', 2017. URL: https://www.space.com/36358-old-satellite-destined-for-graveyard-orbit.html.

[31] T. Li, K. Li, and L. Chen. Maneuver Detection Method Based on Probability Distribution Fitting of the Prediction Error. *Journal of Spacecraft and Rockets*, 56:1114–1120, 2019.

[32] S. Mountin. The Legality and Implications of Intentional Interference with Commercial Communication Satellite Signals. *International Law Studies*, 90:101–197, 2014. URL: https://digital-commons.usnwc.edu/cgi/viewcontent.cgi?article=1013&context=ils.

[33] National Research Council Committee for the Assessment of NASA's Orbital Debris Programs. *Limiting Future Collision Risk to Spacecraft*. 2011. doi:10.17226/13244.

[34] H. Noordung. *Das Problem Der Befahrung Des Weltraumsy ("The Problems of Space Travel")*. Schmidt, R.C., Berlin, Germany, 1929.

[35] Northrop Grumman Newsroom. Northrop Grumman Successfully Completes Historic First Docking of Mission Extension Vehicle with Intelsat 901 Satellite, 2020. URL: https://news.northropgrumman.com/news/releases/northrop-grumman-successfully-completes-historic-first-docking-of-mission-extension-vehicle-with-intelsat-901-satellite.

[36] Oxford Reference. Sidereal Day. URL: https://www.oxfordreference.com/view/10.1093/oi/authority.20110803100504691.

[37] N.V. Patel. Boeing and DirecTV are scrambling to move a satellite before it explode, 2020. URL: https://www.technologyreview.com/2020/01/27/304868/boeing-and-directv-are-scrambling-to-move-a-satellite-before-it-explodes/.

[38] Russell P Patera. Space Event Detection Method. *Journal of Spacecraft and Rockets*, 45(3):554–559, 5 2008. doi:10.2514/1.30348.

[39] S. Pinnagoda. Harmful Interference and Infringements of the Radio Regulations, 2015. URL: https://www.itu.int/en/ITU-R/terrestrial/workshops/RRS-15-Asia/Documents/Harmful%20Interference.pdf.

[40] Rhodes, B.C. PyEphem: Astronomical Ephemeris for Python, 2011.

[41] T.G. Roberts. Popular Orbits 101, 2017. URL: https://aerospace.csis.org/aerospace101/popular-orbits-101/.

[42] T.G. Roberts. Unusual Behavior in GEO: Luch (Olymp-K), 2021. URL: https://aerospace.csis.org/data/unusual-behavior-in-geo-olymp-k/.

[43] T.G. Roberts. Unusual Behavior in GEO: SJ-17, 2021. URL: https://aerospace.csis.org/data/unusual-behavior-in-geo-sj-17/.

[44] T.G. Roberts and C. Bullock. A sustainable geostationary space environment requires new norms of behavior. *MIT Science Policy Review*, 1:34–38, 2020.

[45] T.G. Roberts and R. Linares. Satellite Repositioning Maneuver Detection in Geosynchronous Orbit Using Two-line Element (TLE) Data. In *International Astronautical Congress*, 2020.

[46] Mike Safyan, Jonathan Rosenblatt, and George John. Exhibit 1: Request for Special Temporary Authority, 2020. URL: https://fcc.report/IBFS/SAT-STA-20200119-00011/2171055.

[47] Secure World Foundation (SWF), Center for Strategic and International Studies (CSIS), and the University of Texas at Austin's Department of Aerospace Engineering and Engineering Mechanics. Satellite Dashboard, 2021. URL: https:

//satellitedashboard.org/?satids=858,10000,11648,11964,24932,26824,27509,27632,28644,28903,29163,33414,34713,40258,41308,41838,44625.

[48] C. Shabarekh, J. Kent-Bryant, G. Keselman, and A. Mitidis. A Novel Method for Satellite Maneuver Prediction. In *Advanced Maui Optical and Space Surveillance Technologies Conference*, Maui, Hawaii, 2016. URL: https://amostech.com/TechnicalPapers/2016/SSA/Shabarekh.pdf.

[49] E.M. Soop. *Handbook of Geostationary Orbits*. Doredrecht, Netherlands, 1994.

[50] S.V. Stehman. Selecting and interpreting measures of thematic classification accuracy. *Remote Sensing of Environment*, 62:77–89, 1997.

[51] K. Tsiolkovsky. *Грёзы о Земле и небе ("Dreams of the Earth and the Sky")*. Goncharov, A.N., Moscow, Russia, 1895.

[52] Union of Concerned Scientists. Satellite Database, 2021. URL: http://www.ucsusa.org/nuclear-weapons/space-weapons/satellite-database#.Wf49LGhSz-i.

[53] U.S. Space Force 18th Space Control Squadron. Space-Track.org. URL: https://www.space-track.org/.

[54] D.A. Vallado. *Fundamentals of Astrodynamics and Applications*. Microcosm, Hawthrone, California, 4th edition, 2013.

[55] D.A. Vallado, P. Crawford, R. Hujsak, and T.S. Kelso. Revisiting Spacetrack Report 3. In *AIAA/AAS Astrodynamics Specialist Conference*, Keystone, Colorado, 2006.

[56] S. Zhao and J. Zhang. Minimum-fuel station-change for geostationary satellites using low-thrust considering perturbations. *Acta Astronautica*, 127:296–307, 2016. doi:10.1016/j.actaastro.2016.05.028.